Universiteit Antwerpen

This item is the archived peer-reviewed author-version of:

Stem-cell-derived human microglia transplanted in mouse brain to study human disease

Reference:
Mancuso Renzo, Van den Daele Johanna, Fattorelli Nicola, Wolfs Leen, Balusu Sriram, Burton Oliver, Liston Adrian, Sierksma Annerieke, Fourne Yannick, Poovathingal Suresh, ...- Stem-cell-derived human microglia transplanted in mouse brain to study human disease
Nature neuroscience - ISSN 1097-6256 - 22:12(2019), p. 2111-2116
Full text (Publisher's DOI): https://doi.org/10.1038/S41593-019-0525-X
To cite this reference: https://hdl.handle.net/10067/1738740151162165141

uantwerpen.be
Institutional repository IRUA

Stem cell derived human microglia transplanted in mouse brain to study human disease

Renzo Mancuso[1,2,6,*], Johanna Van Den Daele[2,3,6], Nicola Fattorelli[1,2,6], Leen Wolfs[1,2], Sriram Balusu[1,2], Oliver Burton[1,2], Adrian Liston[1,2], Annerieke Sierksma[1,2], Yannick Fourne[1,2], Suresh Poovathingal[1,2], Amaia Arranz-Mendiguren[1,2], Carlo Sala Frigerio[1,2], Christel Claes[2,3], Lutgarde Serneels[1,2], Tom Theys[5], V. Hugh Perry[4], Catherine Verfaillie[3], Mark Fiers[1,2], Bart De Strooper[1,2,4,*].

[1] Centre for Brain and Disease Research, Flanders Institute for Biotechnology (VIB), Leuven, Belgium

[2] Department of Neurosciences and Leuven Brain Institute, KU Leuven, Leuven, Belgium

[3] Department of Development and Regeneration, Stem Cell Biology and Embryology, KU Leuven Stem Cell Institute, Leuven, Belgium

[4] UK Dementia Research Institute at UCL, University College London, London, UK

[5] Department of Neurosciences, Research group experimental neurosurgery and neuroanatomy, KU Leuven, Leuven, Belgium

[6] Joint first authors

[*] Corresponding authors

Abstract

While genetics highlight the role of microglia in Alzheimer's disease (AD), one third of putative AD-risk genes lack adequate mouse orthologs. Here, we successfully engraft human microglia derived from embryonic stem cells in the mouse brain. The cells recapitulate transcriptionally human primary microglia *ex vivo* and show expression of human specific AD-risk genes. Oligomeric Amyloid-β induces a divergent response in human vs. mouse microglia. This model can be used to study the role of microglia in neurological diseases.

Introduction

Forty-one percent of human genes lack convincing 1:1 mouse orthologs, complicating modelling diseases in mice[1]. We focused on 44 genome-wide significant genetic loci ($p < 5x10\text{-}8$) identified by different AD GWAS studies and selected the genes nearest to the lead SNP to build a list of candidate AD-risk genes[2–4] (Figure 1a, Supplementary Table 1). We found that 15 of these genes lacked a clear 1:1 mouse ortholog (Figure 1b), e.g. *CR1* or *APOC*. Other genes, such as *CD33* and the *MS4A4*-cluster have many-to-many orthology with low protein sequence similarity, suggesting functional divergence. Nine additional AD-risk genes are <60% identical to their mouse ortholog[1], including *TREM2*. Even the largest AD genetic risk factor, the *APOE* polymorphism, does not exist in rodents. In addition, current *in vitro* systems to model human microglia display artificially induced transcriptional signatures[5], limiting their use in disease modelling.

Here, we investigated survival, integration and transcriptomic features of *human* microglia transplanted in mouse brain.

Results

ESC-derived microglia survive and integrate in the mouse brain

We differentiated H9 embryonic stem cell (ESC) into microglia using cytokines CSF1, IL-34, TGF-β and CX3CL1 (Supplementary Figure 1)[6], and transplanted them into the brain of *Rag2*$^{-/-}$ *Il2rγ*$^{-/-}$ *hCSF1*^{KI} mice (*hCSF1*^{KI}) at P4[7]. We created a permissive environment for human microglia integration by pre-treating the neonates with Colony-Stimulating Factor 1-Receptor (CSF1R) inhibitor BLZ945[8], removing an average of 53±7% of host microglia (Supplementary Figure 2). After 8 weeks, H9-microglia, representing 9±5% of the total microglial population (Extended Data

1), showed a mosaic distribution across multiple areas of the brain (Figure 1c and d; Extended Data 2), with nearest neighbour distance[9] and density in transplanted areas similar to host mouse cells (n=4, Figure 1e). H9-microglia showed a complex ramified morphology and expressed homeostatic markers TMEM119 and P2RY12 (Figure 1d-g).

ESC-derived microglia mimic primary human cells at the transcriptome level

We compared the single cell transcriptomic profile of 2,246 transplanted H9-microglia (*in vivo)* (n=3/1: 3 mice in 1 combined sequencing pool), versus 4496 H9-derived monocytes (n=2/1: 2 differentiations in 1 combined sequencing pool) and 3385 microglia *in vitro* (n=2/1), and 22,846 human primary microglia obtained from cortical surgical resections (n=7/7; Extended Data 3; Supplementary Table 2; online Methods and Reporting Summary). We excluded B- and NK/T-cells (316), oligodendrocytes (1159), cycling cells (60), and doublets (172) (Figure 2a-c, Extended Data 3). Using Seurat, we defined 6 main clusters named *In vitro*-1 Monocytes (MNC), *In vitro*-2 Microglia (MG), *In vivo*-Homeostatic Microglia (HM), Cytokine Response Microglia (CRM), CNS-Associated Macrophages (CAM)[10], and Neutrophils (Nφ) (Figure 2a; Extended Data 3), based on experimental data[11] and meta-analysis from microglial transcriptional profiles[12]. CRM represents a novel cluster and is defined by an upregulation of genes encoding cytokines/chemokines (Extended Data 3; Supplementary Table 3). More than 97% of the *in vitro* derived H9-monocytes and microglia were present in *In vitro* clusters (Figure 2a-c), whereas 79% primary microglia isolated from human brain and 60% of transplanted H9-microglia distributed into the *In vivo*-HM cluster (Figure 2a-c; Extended Data 3d and e). A smaller percentage (13%) of primary compared to H9 transplanted microglia (35%) were present in the *In vitro* clusters. In addition, some cells showed a CNS-associated macrophage (CAM) expression profile (Figure 2a and e). Immunohistochemistry and *in situ* hybridization confirmed that CAM cells were in proximity to blood vessels and expressed the perivascular macrophage marker *MRC1* (Figure 2e, lower panels). The engrafted H9 cells expressed the microglia markers *CX3CR1* and *P2RY12* (Figure 2e, upper panels).

Direct comparison between experimental groups revealed that *in vitro* monocytes/microglia displayed >300 differentially expressed genes (logFC>0.2) compared to microglia from surgical samples, consistent with an “activated” profile (Figure 2d and f; Extended Data 4; Supplementary Table 3). In contrast, engrafted H9-microglia displayed a comparable homeostatic signature to that of the cells isolated from the human brain, with only 41 differentially expressed genes (Figure 2d

and g; Extended Data 4a and b). Therefore, the mouse CNS environment is sufficient to drive microglia from an artificial *in vitro* "activated" towards a more natural homeostatic brain resident phenotype.

Human ESC-derived and host mouse microglia display a divergent response to oligomeric Aβ

We tested our humanized system with an acute AD-related challenge, i.e. oligomeric $A\beta_{42}$ (oAβ), previously shown to induce cognitive alterations[13] (Extended Data 5). Mice were injected in the ventricle with 5 µM oAβ (n=3) or scrambled peptide (Scr, n=3) at 8-10 weeks post transplantation. We isolated 4880 transplanted H9-microglia 6 hours after injection (n=3x2/2), excluding CNS-associated macrophages and cycling cells (Extended Data 6). Clustering analysis revealed a homeostatic (H9.HM), a "primed" (H9.PM), and a cytokine (H9.CRM) cluster (Figure 3a; Extended Data 7). The H9.HM cluster was significantly enriched with scrambled peptide treated cells (68%, Chi^2-test, p-value<$2.2x10^{-250}$) and showed high expression of multiple homeostatic genes (Figure 3a; Extended Data 7; Supplementary Table 3). The "primed" H9.PM cluster was very different from the previously characterized activated response (ARM) response in wild type mouse microglia[11] as it expresses an unusual mixture of homeostatic and activation genes[11], and consisted of a larger proportion of scrambled (65%) vs. oAβ cells (35%, Chi^2 test, p-value<10^{-250}) (Figure 3a and b; Extended Data 7). Finally, the H9.CRM cluster was significantly enriched in cells from oAβ treated mice (75%, Chi^2 test, p-value<2.210^{-250}), and displayed high levels of multiple inflammatory cytokines and chemokines, such as *IL1B, IL6, CCL2, CCL4*, etc. (Figure 3a and b; Extended Data 7). Trajectory analysis[14] revealed a phenotypical change of H9-microglia from homeostatic towards the cytokine-response state (Figure 3b; Extended Data 7) with microglia from the H9.PM cluster enriched in the initial and middle phases, indicating they might represent an early response to the injection of peptides (Figure 3b; Extended Data 7).

At the same time, we isolated and sequenced 9942 host mouse microglia (after exclusion of CNS-associated macrophages and other immune or cycling cells) from the same animals to compare their reaction to that of H9-microglia (Figure 3c and d; Extended Data 6). Whereas we acknowledge that the genetic background of the host might cause (unknown) developmental abnormalities, analysis of different wild-type mouse microglial datasets did not reveal expression of *Rag2 or Il2ry*[15] and, although the effect of *Il2ry* deficiency on microglia is not documented, *Rag2* deficiency does not affect microglial number, morphology or gene expression profiles[16]. Clustering analysis yielded a homeostatic (ms.HM), a cytokine (ms.CRM), and an activated (ms.ARM)

response cluster. The HM cluster was significantly enriched with control cells (70%), whereas the CRM and ARM clusters mostly consisted of cells from the mice treated with oAβ, (69% and 77%, Chi^2 test, p-value<10^{-250}) (Figure 3d; Extended Data 8). The ARM cluster showed a similar profile to that of microglia responding to amyloid plaques[11] (Figure 3c and d; Extended Data 8). Trajectory analysis showed that mouse microglia transition from homeostatic to cytokine-response to activated-response cells (Figure 3c; Extended Data 8), suggesting that they form a single successive response of mouse microglia to oAβ. We also assessed whether the CRM transcriptomic signature identified here is uniquely elicited by oAβ, as it has not yet been described in the response to Aβ plaques[11,15] (Supplementary Table 3). Reanalysis of previous data on microglial cells from 3 to 21 months old $APP^{NL\text{-}G\text{-}F}$ mice revealed a small number of cells, previously embedded in the ARM cluster, that displayed a CRM profile (Extended Data 9a-c). In addition, these cells were positioned in the early ARM phase of the trajectory analysis, suggesting that they are part of a common early response to both oAβ and Aβ plaques (Extended Data 9d). We acknowledge that the current work only provides proof of concept, while further more systematic work is ongoing to fully dissect the acute and chronic responses of mouse and human microglia to oAβ and Aβ plaques.

We finally evaluated whether this chimeric model covers the human expressome better than the classical mouse models. We extracted 10,914 one-to-one, bidirectional orthologs between mouse and human (Supplementary Table 2)[1,17] and performed a correlation analysis comparing log-fold changes in gene expression in the CRM vs HM comparison done in each species (FRD < 0.05). We observed a significant, but rather limited correlation in the response to oAβ (R=0.4, Pearson correlation, p-value ≈ 0) with a number of genes changed in mouse or human alone (logFC > 0.2; Figure 3e; Extended Data 10), 207 of them showing opposite behaviour (Figure 3f; Extended Data 10c), such as *TYMP*, *NFKB, PPARG, LIMK2* and *TGFBR1,* a homeostatic microglia marker in mouse[18] (Extended Data 10c), and the AD-risk genes *ABI3, BIN1* and *PICALM* (Figure 3f). We also explored how the 8266 human genes with no clear mouse ortholog reacted to oAβ and found 79 and 127 uniquely up- and down-regulated human genes, mainly involved in cytokine/chemokines responses (Extended Data 10d and e). The human response was particularly strong for *IL1B* and *CCL2* (Figure 3e, red arrows), which have been experimentally implicated in the pathology of AD[19,20] (Figure 3e, Extended Data 10). Remarkably, 12 of the 15 AD-risk genes identified as lacking 1:1 mouse orthologs (in Figure 1a), were expressed in primary microglia from surgical samples (Figure 3g), confirming the association of genetic risk of AD with microglia. Reassuringly, all these genes were also detected in the transplanted human H9-microglia (including *APOC*, *CD33*, *CR1*, *MS4A* and *TREM2*). The similarities in gene expression between $Rag^{-/-}$ $Il2r\gamma^{-/-}$

and wild type mouse microglia (Figure 3g) further supports the proof of concept study presented here.

Discussion

Although *in vitro* studies may provide some mechanistic insights into the function of human microglia, it is also clear that signals from the CNS microenvironment are required to sustain microglial specification, and that a loss of those cues dramatically disrupts the microglia phenotype driving them towards an activated state[5]. In addition, some AD-linked genes (e.g TREM2-membrane phospholipids/APOE, CD33-sialic acid, etc.) play a role in the cross-talk between microglia and other brain cells. The main challenge is to understand this cellular phase of AD[21] and therefore introducing those complex aspects into a model of disease is extremely important. We present here a novel model using ESC-derived human microglia transplantation into the mouse brain providing the human cells with the crucial environment that defines microglial identity. Given the limited similarity between mouse and human microglia in terms of candidate AD-risk genes, this model provides a very useful alternative to study the response of human microglia *in vivo* in the context of AD and other diseases affecting the CNS, opening important new routes to understand the role of the many genes identified in the GWAS and other genetic studies which are not well modelled in mouse cells.

ESC-derived human microglia transplanted into mouse brain represents clearly a step forward to model part of the GWAS defined risk of AD. Despite certain limitations that should be considered (e.g. lack of adaptive immune system, variability in the grafting efficiency of different pluripotent stem cells, iPSC), we anticipate that our approach will be widely applicable to study other neurological diseases. The use of human H9 cells in combination with CRISPR/Cas9 technology opens unanticipated possibilities to model human specific genetic aspects of brain disease.

Acknowledgments

Work in the De Strooper laboratory was supported by the European Union (ERC- 834682 - CELLPHASE_AD), the Fonds voor Wetenschappelijk Onderzoek (FWO), KU Leuven, VIB, UK-DRI (Medical Research council, ARUK and Alzheimer Society), a Methusalem grant from KU Leuven and the Flemish Government, Vlaams Initiatief voor Netwerken voor Dementie Onderzoek (VIND, Strategic Basic Research Grant 135043) , the "Geneeskundige Stichting Koningin Elisabeth", Opening the Future campaign of the Leuven Universitair Fonds (LUF), the Belgian Alzheimer Research Foundation (SAO-FRA) and the Alzheimer's Association USA. Bart De Strooper is holder of the Bax-Vanluffelen Chair for Alzheimer's Disease. He receives funding from MRC, the Alzheimer Society and Alzheimer's Research UK via the Dementia research institute. Cell sorting was performed at the KU Leuven FACS core facility, and sequencing was carried out by the VIB Nucleomics Core. Renzo Mancuso is recipient of a postdoctoral fellowship from the Alzheimer's Association, USA.

Authors contribution

R.M. conceived and designed the study, performed all the experiments and wrote the manuscript. J.V.D.D. conceived and designed the study, performed all the experiments and wrote the manuscript. N.F. conceived and designed the study, performed all the experiments and wrote the manuscript. L.W. performed all the experiments. S.B. contributed on the preparation of oligomeric amyloid beta and intracerebral injections. O.B. assisted with the flow cytometry experiments. A.L. contributed on the interpretation of the data. A.S. assisted on human genetics and human to mouse orthology. Y.F. assisted with the analysis of single cell RNA sequencing data. S.P. assisted with the single cell RNA sequencing experiments. A.A.M. optimized the xenograft experiments. C.S.F. optimized the single cell sequencing experiments and library preparations. C.C. assisted with the differentiation of microglia from embryonic stem cells. L.S. established and maintained the mouse colonies. T.T. recruited the human subjects, performed the neurosurgeries and provided the human tissue specimens. V.H.P. contributed to the design of the study and interpretation of the data. C.V. contributed to the design of the study and interpretation of the data. M.F. contributed to the design of the study, and analysis and interpretation of the data. B.D.S. conceived and designed the study, and wrote the manuscript. All authors discussed the results and commented on the manuscript.

Competing interest statement

The authors do not have conflicts of interest to disclose with the current study. BDS receives grants from different companies that support his research and is a consultant for several companies but nothing is directly related to the current publication.

References (for main text only)

1. Zerbino, D. R. *et al.* Ensembl 2018. *Nucleic Acids Res.* **46,** D754–D761 (2018).

2. Jansen, I. E. *et al.* Genome-wide meta-analysis identifies new loci and functional pathways influencing Alzheimer's disease risk. *Nat. Genet.* 1 (2019). doi:10.1038/s41588-018-0311-9

3. Lambert, J. C. *et al.* Meta-analysis of 74,046 individuals identifies 11 new susceptibility loci for Alzheimer's disease. *Nat. Genet.* **45,** 1452–1458 (2013).

4. Kunkle, B. W. *et al.* Genetic meta-analysis of diagnosed Alzheimer's disease identifies new risk loci and implicates Aβ, tau, immunity and lipid processing. *Nat. Genet.* **51,** 414–430 (2019).

5. Bohlen, C. J. *et al.* Diverse Requirements for Microglial Survival, Specification, and Function Revealed by Defined-Medium Cultures. *Neuron* **94,** 759–773.e8 (2017).

6. Claes, C. *et al.* Human stem cell–derived monocytes and microglia-like cells reveal impaired amyloid plaque clearance upon heterozygous or homozygous loss of TREM2. *Alzheimer's Dement.* 1–12 (2018). doi:10.1016/j.jalz.2018.09.006

7. Rathinam, C. *et al.* Efficient differentiation and function of human macrophages in humanized CSF-1 mice. *Blood* **118,** 3119–3128 (2011).

8. Hagemeyer, N. *et al.* Microglia contribute to normal myelinogenesis and to oligodendrocyte progenitor maintenance during adulthood. *Acta Neuropathol.* **134,** 441–458 (2017).

9. Davis, B. M., Salinas-Navarro, M., Cordeiro, M. F., Moons, L. & Groef, L. De. Characterizing microglia activation: A spatial statistics approach to maximize information extraction. *Sci. Rep.* **7,** 1–12 (2017).

10. Jordão, M. J. C. *et al.* Single-cell profiling identifies myeloid cell subsets with distinct fates during neuroinflammation. *Science (80-.).* **363,** (2019).

11. Sala Frigerio, C. *et al.* The major risk factors for Alzheimer's disease: Age, Sex and Genes, modulate the microglia response to Aβ plaques. *Cell Rep.* **In Press,** 1293–1306 (2019).

12. Friedman, B. A. *et al.* Diverse Brain Myeloid Expression Profiles Reveal Distinct Microglial Activation States and Aspects of Alzheimer's Disease Not Evident in Mouse Models. *Cell Rep.* **22,** 832–847 (2018).

13. Brouillette, J. *et al.* Neurotoxicity and Memory Deficits Induced by Soluble Low-Molecular-Weight Amyloid-1-42 Oligomers Are Revealed In Vivo by Using a Novel Animal Model. *J. Neurosci.* **32,** 7852–7861 (2012).

14. Trapnell, C. *et al.* The dynamics and regulators of cell fate decisions are revealed by pseudotemporal ordering of single cells. *Nat. Biotechnol.* **32,** 381–386 (2014).

15. Keren-Shaul, H. *et al.* A Unique Microglia Type Associated with Restricting Development of Alzheimer's Disease. *Cell* **169,** 1276–1290.e17 (2017).

16. Marsh, S. E. *et al.* The adaptive immune system restrains Alzheimer's disease pathogenesis by modulating

microglial function. *Proc. Natl. Acad. Sci.* **113,** E1316–E1325 (2016).

17. Shay, T. *et al.* Conservation and divergence in the transcriptional programs of the human and mouse immune systems. *Proc. Natl. Acad. Sci.* **110,** 2946–2951 (2013).

18. Butovsky, O. *et al.* Identification of a unique TGF-β-dependent molecular and functional signature in microglia. *Nat. Neurosci.* **17,** 131–143 (2014).

19. Bhaskar, K. *et al.* Regulation of tau pathology by the microglial fractalkine receptor. *Neuron* **68,** 19–31 (2010).

20. Deshmane, S. L., Kremlev, S., Amini, S. & Sawaya, B. E. Monocyte Chemoattractant Protein-1 (MCP-1): An Overview. *J. Interf. Cytokine Res.* **29,** 313–326 (2009).

21. De Strooper, B. & Karran, E. The Cellular Phase of Alzheimer's Disease. *Cell* **164,** 603–615 (2016).

Figure legends (for main text only)

Figure 1. Human ESC-derived microglia successfully engraft the mouse brain. (a) Selection of 44 genes with $p>5x10^{-8}$ from 3 landmark studies in the field. See online methods. **(b)** From these 44 candidate AD risk genes[3,4,8], 15 (marked with a red dot) do not have a clear 1:1 mouse ortholog or display <60% identity between human and mouse at the primary amino acid sequence. Colour scale, green (high similarity) to red (low similarity). (**c**) Schematic representation of the area of mouse brain covered by transplanted human microglia. Microglia are represented by green dots, and the distance between anatomically consecutive sections is 500µm. (**d**) H9-microglia successfully engraft the mouse brain and (**e**) express homeostatic markers TMEM119 and P2RY12 (n=4 mice). Scale bars of 100 and 5µm, respectively. (**f**) Transplanted cells distribute across the parenchyma forming a mosaic with similar nearest neighbour distance (NND) and density to that of mouse cells from adjacent areas (n=4 mice per group, two-tailed t-test p=0.9, graph shows mean±SEM). H9-microglia are labelled in green ($Iba1^+$ GFP^+), whereas arrowheads highlight few mouse cells ($Iba1^+$ GFP^-) co-existing with H9-microglia in the grafted areas of the parenchyma (n=4 mice). Scale bar, 100 µm. (**g**) Higher magnification microphotographs and 3D reconstruction by Imaris show typical morphology with high complexity branching in H9-microglia (n=4 mice). Scale bar 5 µm.

Figure 2. H9-microglia isolated 8 weeks after transplantation are similar to human primary microglia. (a) t-SNE plot visualizing 33,144 single cells sorted based on CD11b (primary human), CD11b hCD45 and GFP (engrafted H9-microglia) staining, and *in vitro* derived monocytes (MNC) and microglia (MG) after quality control, and removal of peripheral cells, cycling cells and doublets. Cells are coloured according to clusters identified with Seurat's kNN and merging: *In vitro*-1 MNC, *In vitro*-2 MG, *In vivo*-Homeostatic Microglia (HM) and Cytokine Response Microglia (CRM), CNS-Associated Macrophages (CAM)[10], and Neutrophils (Nφ). The assignment of different clusters to distinct cell types/states is based on previous experimental data from our lab[11] and a recent meta-analysis describing multiple modules of microglial transcriptional profiles[12], as detailed in Extended Data 4a-c and Supplementary Table 3. (**b, c)** Distribution and percentage of cells from either *in vitro*, *in vivo* (engrafted) H9 or primary human microglia across the different clusters identified. (**d**) Most highly expressed genes in the different samples: *in vitro-1* MNC; *in vitro-2* MG, *in vivo* (engrafted) H9 and primary microglia. (**e**) *In situ* hybridization for *CX3CR1* and *P2RY12* (microglia) and *MRC1* (perivascular macrophages) confirming the location of the two main distinct identities acquired by H9 engrafted cells (GFP) in the mouse brain (n=4 mice). Scale bar is

25 μm and 10 μm in the left and right panels, respectively. (**f, g**) Volcano plots showing gene expression differences between average gene expression in (**f**) 22,846 primary vs. 3385 *in vitro* MG and (**g**) 22,846 primary vs. 2,246 engrafted H9-microglial cells (with a logFC threshold of 0.2, Wilcoxon Rank Sum test, *p-values* adjusted with Bonferroni correction based on the total number of genes in the dataset). Genes associated to homeostatic or activation expression profiles are highlighted in blue and red, respectively (Supplementary Table 3).

Figure 3. Human and host mouse microglial response to oligomeric Aβ. (**a, b**) Analysis of the response of H9-microglia upon oAβ exposure. (**a**) t-SNE plot visualizing the 4880 H9 microglia passing quality control, and after removal of CAM, cycling cells and doublets. Cells are coloured according to clusters identified with Seurat's kNN (upper panel; H9.HM: Homeostatic Microglia, H9. PM: Primed Microglia, H9.CRM: Cytokine Response Microglia, H9) and treatment (lower panel; Scr: scrambled peptide, oAβ: oligomeric Ab). (**b**) Plot of the phenotypic trajectory followed by H9-microglia upon oligomeric Aβ exposure, obtained by an unbiased pseudotime ordering with Monocle 2 and coloured by clusters as in **d**. H9-microglia followed a trajectory from H9.HM and H9.PM, to H9.CRM. The heatmap shows the differential expression of representative genes from each cluster, ordered by pseudotime. (**c, d**) Analysis of the response of endogenous (*Rag2*$^{-/-}$ *Il2rγ*$^{-/-}$) mouse microglia upon oligomeric Aβ challenge. (**d**) t-SNE plot visualizing the 9942 endogenous mouse microglia passing quality control, and after removal of peripheral cells, CNS-Associated Macrophages (CAM) cycling cells and doublets. Cells are coloured according to clusters identified with Seurat's kNN (upper panel; ms.HM: (mouse) Homeostatic Microglia, ms.CRM: Cytokine Response Microglia, ms.ARM: Activated Response Microglia) and treatment (lower panel; Scr: scrambled peptide, oAb: oligomeric Ab). (**c**) Plot of the phenotypic trajectory followed by endogenous mouse microglia upon oligomeric Aβ exposure, obtained by an unbiased pseudotime ordering with Monocle 2 and coloured by clusters as in **a**. Mouse microglia followed a trajectory from ms.HM to ms.CRM to ms.ARM. The heatmap shows the differential expression of representative genes from each cluster, ordered by pseudotime. (**e**) Correlation analysis of the log-fold change (logFC) in H9 (y-axis) and host (*Rag2*$^{-/-}$ *Il2rγ*$^{-/-}$) mouse (x-axis) microglia upon oligomeric Aβ challenge relative to scrambled peptide (Pearson correlation, R=0.4. Differentially expressed genes are highlighted in green when significant in both species, blue only in H9-microglia or orange only in mouse microglia. Numbers between brackets in the legend represent the amount of up and downregulated genes in each group, respectively. (**f**) Expression changes induced by Aβ challenge in the selected candidate AD-risk genes (Figure1b). (**g**) Extension of the table shown in Figure 1a highlighting the important number of putative AD-risk genes in humans that

lack good orthologues in mice or show an opposite behaviour upon Aβ challenge (highlighted by red dots). Expression profile of 44 putative AD genes in our datasets (H9-microglia; primary human microglia from 7 patients; and mouse host *Rag2*$^{-/-}$ *Il2rγ*$^{-/-}$microglia, mouse RM), and wild type mouse microglia from 2 independent datasets of 12-week-old immunocompetent C57Bl/6 mice (Sala Frigerio et al.,[11] , SF; and Keren-Shaul et al., KS[15]). We identified 15 genes with observed expression in human but not mouse microglia and, that were also observed in H9-microglia.

Tables

Supplementary Table 1. Human to mouse orthology for Alzheimer's Disease risk genes.

Supplementary Table 2. Clinical information of the human specimens.

Supplementary Table 3. Gene expression scores.

Supplementary Table 4. List of human-mouse orthologs.

Methods (online)

Sample size was estimated based on previous experiments performed in the lab[11]. No samples were excluded from the analysis and all attempts at replication were successful. The experimental groups were ramdomised to avoid gender, litter and cage effects. Investigators were blinded when performing all experiments

Human vs. mouse gene orthology and selection of putative AD-risk genes

We determined the orthology between human and mouse genomes using Ensembl Biomart[1]. We defined "good orthology" as every gene with one-to-one, bidirectional orthology between the two species and >60% protein sequence similarity. This resulted in a total of 10,914 genes. The full list is shown in Supplementary Table 3.

We based our selection of putative AD-risk genes on several recent publications[2–4]. We focused on 44 genome-wide significant loci ($p<5x10-8$) described in these publications and selected as being the nearest gene to the lead SNP. We used the union of these gene sets for our analysis. In summary, we extracted 23 genes from Lambert et al. (Table 2 of the original report)[3], 33 genes from Jansen et al. (Table 1of the original report)[2] and 21 genes from Kunkle et al. (Table 1 of the original report)[4]. Figure 1a shows the distribution of these genes across the different reports and illustrates how they overlap.

In vitro generation of microglia from ESCs

In vitro microglia differentiation from embryonic stem cells was based on previously described protocols[6]. On days 17, 21, 25, 28, and 32, non-adherent cells were harvested and selected using CD14-labelled magnetic beads (Miltenyi) following manufacturer specifications. Briefly, cells were collected and centrifuged for 5 min at 300g. Then, cells were incubated for 15 min at 4°C in 80 µl MACS buffer (AUTOMACS + 5% MACS serum, Miltenyi) with 20 µl of CD14-beads (Miltenyi), and passed through a LS column (QuadroMACS, Miltenyi). The CD14+ fraction was collected and centrifuged for 5min at 300g. Monocytes were then differentiated into microglia-like cells using microglia differentiation medium (TIC) (DMEM/F12, Glutamine (2mM), N-Acetyl Cysteine (5µg/mL), Insulin (1:2000), Apo-Transferrin (100 µg/mL), Sodium Selenite (100 ng/mL), Cholesterol (1.5 µg/mL), Heparan Sulphate (1 µg/mL)) supplemented with 50 ng/ml IL34, 50

ng/mL M-CSF, 10 ng/ml CX3CL1 and 25 ng/mL TGF-β, based on Abud et al. (2017)[22]. The medium was changed every other day.

Mice

Rag2$^{-/-}$ *IL2rγ*$^{-/-}$ *hCSF1*^{KI} mice were purchased from Jacksons Labs (strain 017708), and bred and maintained in local facilities. All the experiments were performed in these mice as human microglia require hCSF1 for their growth and survival[7]. Mice were housed in groups of 2-5, under a 14 h light/10 h dark cycle at 21°C, with food and water *ad libitum*. All experiments were conducted in 8-12 weeks old male and female according to protocols approved by the local Ethical Committee of Laboratory Animals of the KU Leuven (government licence LA1210591, ECD project number P177/2017) following local and EU guidelines.

Endogenous mouse microglia depletion

The CSF1R inhibitor BLZ945 was dissolved in 20% (2-hydroxypropyl)-β-cyclodextrin (Sigma-Aldrich). Newborns were injected (i.p.) 24 and 48h prior to human cell transplantation at a dose of 200 mg/kg bodyweight.

Transplantation of human microglia into the mouse brain

Grafting of human PSC-derived microglia was performed as previously described[23]. Briefly, human microglia were dissociated and suspended at a concentration of 100,000 cells/µl in PBS. At P4, mice were anaesthetized by hypothermia and bilaterally injected with 1µl of cell suspension at coordinates from Bregma: anteroposterior, -1mm; lateral, ±1mm. After the injections, mice were allowed to recover on a heating pad at 37°C, and then transferred back to their cage.

Isolation of human primary microglia

Human primary microglia were isolated from brain tissue samples resected from the temporal cortex during neurosurgery. All samples represented lateral temporal neocortex and were obtained from patients who underwent amygdalo-hippocampectomy for medial temporal lobe seizures. The mesial temporal specimens were sent to pathology and thus not available for study purposes.

Samples were collected at the time of surgery and immediately transferred to the lab for tissue processing, with post sampling intervals of 5-10 min. All procedures were conducted to protocols approved by the local Ethical Committee (protocol number S61186).

Preparation and intracerebral injection of oligomeric amyloid

Oligomeric Aβ 1-42 (oAβ, 5µl 10µM) or scrambled peptide (Scr, 5µl 10µM) were prepared as previously described by Kuperstein et al.[24] Briefly, recombinant amyloid beta 1-42 peptide (rPeptide; #A-1163-1) or scrambled amyloid beta 1-42 (rPeptide; #A-1004-1) were thawed at room temperature 30 minutes before preparation. Peptides were solubilized in 99% hexafluoroisopropanol (HFIP) (Sigma-Aldrich; #105228) at 1 mg/ml concentration. The HFIP was evaporated using a stream of nitrogen gas, the resulting peptide pellet was resolved in dimethylsulfoxide (DMSO; Sigma-Aldrich; #D4540), at final concentration of 1 mg/ml. DMSO was exchanged with Tris-EDTA (50 mM Tris and 1 mM EDTA, pH 7.5) using 5-ml HiTrapTM desalting columns (GE Healthcare; #17-408-01). The eluted peptide concentration was determined using Bradford reagent (Bio-Rad; #5000006) according to the manufacturer's instructions. The eluted peptide was left to oligomerize at room temperature for two hours in Tris-EDTA buffer. oAβ or scrambled peptide was further diluted to 10 µM in Tris-EDTA buffer and stored at -80^{o}C until use. At 8-10 weeks of age, grafted mice were anesthetized with a ketamine/xylazine mixture (85 and 13 mg/kg), and 5 µl of either oAβ (10 µM) or scrambled peptide (10 µM) were stereotactically injected in the left ventricle at the following coordinates from bregma: anteroposterior, -0.1 mm; mediolateral, +1 mm; dorsoventral, -3 mm. Mice were allowed to recover in a thermo-regulated chamber and then transferred back to their original cage. Isolation of microglia was performed 6h after the intracerebral injection of the peptides.

Isolation of human and mouse microglia from the mouse brain

Mice were terminally anesthetized with an overdose of sodium pentobarbital and transcardially perfused with heparinized PBS. Brains were harvested in PBS 2%, FCS, 2mM EDTA (FACS buffer), mechanically triturated and enzymatically dissociated using the Neural Tissue Dissociation Kit (P) (Miltenyi) following manufacturer specifications. Then, samples were passed through a cell strainer of 70µm mesh (BD2 Falcon) with FACS buffer, and centrifuged twice at 500g for 10 min at 4°C. Next, cells were resuspended in 35% Percoll (GE Healthcare) and centrifuged at 500g for 15

min at 4°C. The supernatant and myelin layers were discarded, and the cell pellet enriched in microglia was resuspended in FcR blocking solution (Miltenyi) in cold FACS buffer, following manufacturer specifications. After a wash, primary antibody labelling was performed for 30 min at 4 °C, using the anti-CD11b (Miltenyi) and anti-hCD45 (BD Bioscience), adding e780 (eBiocience) as a cell viability marker. Moreover, unstained cells and isotype-matched control samples were used to control for autofluorescence and/or non-specific binding of antibodies. Samples were run on a BD FACS Aria II Flow Cytometer and data were analysed using FlowJo and FCS express software. Human cells were sorted according to the expression of CD11b, hCD45, and GFP, whereas mouse cells only expressed CD11b but were negative for hCD45 and GFP (Extended Data 2). For each experimental condition, we pooled the same number of cells from three mice.

Histological analysis

Mice were terminally anesthetized with an overdose of sodium pentobarbital and transcardially perfused with heparinized PBS and 4% PFA in PBS. Brains were harvested, post fixed in 4% PFA overnight, and cut in transverse serial sections (35 μm thick) with a vibrating microtome (Leica). For each sample, 6 series of sections were sequentially collected in free-floating conditions and kept in cryoprotectant solution at −20°C. Sections were blocked with 5% normal serum in PBS-0.2% Tween 20 for nonspecific binding. After rinses with PBS-0.1% Tween 20 (PBST), sections were incubated overnight at 4°C with anti-GFP (Abcam, ab13970), anti-Iba1 (Wako, 019-19741), anti-P2RY12 (Sigma Aldrich, HPA014518) and anti-TMEM119 (Abcam, ab185333). After washes with PBST, sections were incubated with the appropriated biotinylated (Vector Labs) or Alexa 488- and 594-conjugated secondary antibodies (Invitrogen) for 1h at RT. When necessary, sections where incubated with Alexa 488-conjugated Streptavidin (Invitrogen) for 1h at RT. Finally, sections were counterstained with DAPI and mounted with Mowiol/DABCO (Sigma-Aldrich) mixture. Sections were visualized on a Nikon A1R Eclipse confocal system. Nearest neighbour distance (NND) analysis was performed in 20X microphotographs by using a script for Fiji (ImageJ) as previously described by Davis et al. (2017).[9]

Single cell mRNA libraries preparation and sequencing

After microglial isolation, we performed single cell RNA sequencing by using 10X Genomics single cell gene expression profiling kit. cDNA libraries were produced following manufacturer

instructions. cDNA libraries were then sequenced in an Illumina HiSeq platform 4000 with the sequencing specification recommended by 10X Genomics workflow. For each experimental condition, we pooled the same number of cells from three mice.

Human-mouse orthologs

Human to mouse and mouse to human orthologs tables were downloaded from Ensembl/Biomart (release 94)[1]. From these tables, only those genes were extracted that have a clean one-to-one bidirectional ortholog. After filtering out genes that do not express in our human and mouse microglia datasets, the table resulted in 10914 genes (Supplementary Table 4).

Statistics

Analysis of histological data

Nearest neighbor distance (NND) and microglial density data (from Figure 1) were analysed with a two-tailed t-test. Data distribution was assumed to be normal but this was not formally tested. P values < 0.05 were consider statistically significant at a confidence interval of 95%. Data were represented as mean±SEM.

Analysis of single cell RNA sequencing datasets

Alignment. The raw BCL files were demultiplexed and aligned by Cellranger (version 2.1.1) against a human genome database (build hg38 build 84) and mouse database (mm10 build 84). Raw count matrices were imported in R (version 3.4.4) for data analysis.

Quality control of cells - step 1. For each dataset, to exclude poorly sequenced cells, damaged cells and dying cells, we filtered out cells with less than 1000 reads or less than 100 genes detected; moreover, we excluded cells with more than 10% of reads aligning to mitochondrial genes. Cells with a number of reads or genes above 3 standard deviations from the sample mean were considered as doublets and removed. Genes detected in less than 3 cells were excluded from the count matrices. Data were analysed by principal component analysis (PCA) to identify any obvious batch effects. For the joint analysis of H9-derived microglia and primary microglia from surgical resections (Figure 2), the mean depth of sequencing was 102,000 reads/cell, while the mean number of genes detected per cell was 2072. For the analysis of mouse microglia (Figure 3), the mean depth of

sequencing was 68,000 reads/cell, while the mean number of genes detected per cell was 1777. For the analysis of H9-derived microglia (Figure 3), the mean depth of sequencing was 96,000 reads/cell, while the mean number of genes detected per cell was 1964.

Quality control of cells - step 2. We analysed each dataset using the R package Seurat (version 2.3.4)[25] for the mouse and H9-derived microglia datasets, and version 3.0[26] for the joint analysis). We performed principal component analysis (PCA) on both the mouse and H9-derived microglia datasets, after data normalization and scaling and selection of the most variable genes, respectively 2000 and 1390. We selected the first principal components (PCs), 20 for mouse and 20 for H9-derived cells, based on a scree plot (i.e. a plot of the PC eigenvalues in decreasing order) as input for the downstream calculations. Clusters are identified using Seurat's FindClusters function. Further non-linear dimensionality reduction for visualization is done using t-SNE. The standard workflow was followed also for the joint analysis, see Data integration and Joint clustering section.

In the joint dataset integrating in vitro H9 MNC and MG, in vivo H9 microglia and primary microglia from human cases, unbiased clustering by Seurat identified 13 major cellular populations (integrated clustering resolution = 0.8) after removal of B cells (28 cells, marked by *CD52, CD48* expression), NK/T cells (288 cells, marked by *NKG7, CD247, CD7* expression), oligodendrocytes (1159 cells, marked by *MBP, PLP1* expression), cycling cells (60 cells, marked by *TOP2A* expression), doublets (172 cells, co-expressing microglial and neuronal/astrocyte markers) and a microglial cluster with very low number of reads and genes (168 cells, with mean genes = 545.9/cell, mean reads = 967.5/cell), probably reflecting damaged or low-quality cells. Post-QC a total of 32973 microglia, CNS-associated macrophages, monocytes and neutrophils cells were retained for further analysis. Seurat clusters were merged in 6 main cell types/states (Figure 2a) according to transcriptomic profile similarities as indicated by differential expression analyses and signature scoring of cells based on published single-cell microglia datasets (Extended Data 3; Supplementary Table 3). Stability of the clustering was assessed by multiple runs of analysis exploring different combinations of parameters and clusters-correlation analyses, in order to avoid over- or under-clustering of the data.

For the mouse microglia dataset, we identified 12 major cellular populations, most of them showing a tight distribution on the t-SNE plot (Extended Data 6a), with two main clusters (6 and 7) clearly separating, as well as four other very small clusters (9,10,11,12). Clusters 0 to 5 expressed high levels of homeostatic microglia markers, which were not expressed in the other, separated, clusters (Extended Data 6b). Cluster 8 expressed activated microglia and cytokines markers (Extended Data

6b). Based on a panel of marker genes (Extended Data 6c), we could identify enrichment for markers of different cell types other than microglia in the six separated clusters. Clusters 6 and 7 showed high expression levels of gene markers of neutrophils (*Ccrl2*) and monocytes (*Ccr2*), respectively. Clusters 9, 10, and 12, all composed by very small number of cells, expressed gene signatures of other brain cells (astrocytes (*Clu*), neurons (*Npy*), oligodendrocytes (*Mbp*). Cluster 11 was enriched in markers of cycling cells (*Top2a*). Overall, 89% of cells (13342/15036) in our post-QC dataset were microglia, and only these cells were retained for further analysis. The final analysis was performed on oAβ and scrambled peptide-treated cells (Figure 3), consisting of a final dataset of 9942 cells.

For the H9-derived microglia dataset, we identified 8 major cellular populations, distributed in two main groups of cells on the t-SNE plot (Extended Data 6d), both showing a treatment-associated distribution of cells (Extended Data 6e). Clusters 0, 2, 3, 5 expressed homeostatic microglia markers (Extended Data 6f), while clusters 1 and 4 expressed gene markers of CNS-associated macrophages (*MRC1, CD163*). Cluster 7 expressed low level of macrophage markers and some activation markers (*CD74*), while cluster 6 was enriched in markers of cycling cells (*MKI67*). Cluster 8 counted few cells, was very different from all the others and had no clear markers, probably reflecting a small population of doublets. Overall, 72% of cells (6444/8998) in our post-QC dataset were microglia, and only these cells were retained for further analysis. The final analysis was performed on oAβ and scrambled peptide-treated cells (Figure 3), consisting of a final dataset of 4880 cells, after excluding CNS-associated macrophages.

Independent clustering of mouse and H9-derived microglia. Cells passing QC were analysed using functions provided with the Seurat package, version 2.3.4. Data was log normalized and we regressed out the variable of read count. Next, we identified the genes with highest variability and performed PCA on such gene set. We identified the most informative principal components based on a scree plot and we used these to perform cell clustering. Identification of differential expressed genes was performed using the Wilcox test implemented by Seurat's FindMarker. t-SNE plots were prepared using Seurat's t-SNE implementation. For the mouse microglia dataset, we considered 1020 highly variable genes for PCA and the first 15 PCs for clustering. The H9-derived human microglia dataset was analysed similarly as described above, by performing PCA on the 1886 most variable genes and by using the first 15 PCs to perform cluster analysis.

Data integration and joint clustering. Cells passing QC were analysed using the Seurat package, version 3.0. The combined object (H9-derived naive microglia and primary microglia from patients) was split into a list, with each dataset as an element. Standard preprocessing (log-normalization)

was performed individually for each of the two datasets, and variable features (nfeatures = 2000) that were identified based on a variance stabilizing transformation (selection.method = "vst"). Next, we identified anchors using the FindIntegrationAnchors function, giving the list of Seurat objects as input. We used all default parameters, including the dimensionality of the dataset (dims = 1:30). We passed these anchors to the IntegrateData function, in order to get an integrated (or 'batch-corrected') expression matrix for all cells, enabling them to be jointly analysed. We used the new integrated matrix for downstream analysis and visualization using the standard workflow.

Pseudotime analysis. To infer the pseudotime of microglia progression towards phenotypic change in response to oAβ challenge, we used the Monocle 2 package (version 2.6.4)[14,27]. We performed an unsupervised identification of cell trajectories and states, based on the top 200 marker genes identified with a differential expression analysis between oAβ treated cells and scramble-treated cells.

Differential Expression. Differential expression was performed using functions provided with the Seurat package; p values were calculated using the Wilcoxon rank-sum test. In Seurat's function FindAllMarkers, no threshold for the min.pct parameter was applied, in order not to miss marker genes of rare cell populations. All the other parameters were set to default. Genes with adjusted p values (using a Bonferroni correction) < 0.05 were considered significantly differentially expressed. Differential expression was used to find cluster markers in all datasets. For Figure 3, differential expression was performed with the FindMarkers function of Seurat comparing CRM and HM clusters, both in mouse and H9-derived human datasets, with no logFC or min.pct thresholds.

Scores of cell types/states signatures. For Extended Data 3 and 7-9, signatures were calculated using Seurat's *AddModuleScore* function using a list of marker genes identified for each cell type or cell state, based on previous experimental data from our lab[19] and recent description of microglial transcriptional modules[12]. See Supplementary Table 3 for a complete list of all genes defining the different signatures.

Distribution of samples across clusters. We compared the distribution of samples between different clusters by two different tests. We used two-dimensional contingency table (Pearson's Chi-squared test) to test the overall distribution of treatments across clusters (null hypothesis assuming that the joint distribution of the cell counts in a 2-dimensional contingency table is the product of the row and column marginals). In addition, we used goodness-of-fit test (Chi-squared test for given probabilities) to test distribution within each cluster (null hypothesis assuming that the observed

population probabilities in each cluster equal the expected ones; human microglia: Aβ 45.6%, Scr 54.4%; mouse microglia: Aβ 43.8%, Scr 56.2%).

Pathway enrichment analysis. Pathway analysis was performed with GOrilla (Gene Ontology enRIchment anaLysis and visuaLizAtion tool)[28], with single ranked list of genes as running mode. For both mouse and H9-derived microglia, genes were ranked by p-value adjusted taken from the Differential Expression analysis performed between CRM and HM clusters. The enriched ontology terms were then grouped by major functional categories, and the most significant terms (after multiple correction by FDR) in the H9-microglia dataset were compared to the same terms in the mouse host microglia dataset (Extended Data 10a). Each gene that was found significant in Differential Expression was then annotated with the functional categories it belongs to (Extended Data 10b and c), considering only the terms that were found significantly enriched in the GOrilla analysis.

Data availability

The data generated in this study is available from GEO (identifier to be provided). The data and code are also available at scope.bds.org. Data from Karen-Shaul et al.[15] is available from GEO (identifier GSE98969). Data from Sala Frigerio et al. [11] is available from GEO (identifier GSE127893).

Methods-only references

22. Abud, E. M. *et al.* iPSC-Derived Human Microglia-like Cells to Study Neurological Diseases. *Neuron* **94,** 278–293.e9 (2017).

23. Espuny-Camacho, I. *et al.* Hallmarks of Alzheimer's Disease in Stem-Cell-Derived Human Neurons Transplanted into Mouse Brain. *Neuron* **93,** 1066–1081.e8 (2017).

24. Kuperstein, I. *et al.* Neurotoxicity of Alzheimer's disease Aβ peptides is induced by small changes in the Aβ42 to Aβ40 ratio. *EMBO J.* **29,** 3408–3420 (2010).

25. Stuart, T. *et al.* Comprehensive integration of single cell data. *bioRxiv* 1–24 (2018). doi:10.1101/460147

26. Butler, A., Hoffman, P., Smibert, P., Papalexi, E. & Satija, R. Integrating single-cell transcriptomic data across different conditions, technologies, and species. *Nat. Biotechnol.* **36,** 411–420 (2018).

27. Qiu, X. *et al.* Reversed graph embedding resolves complex single-cell trajectories. *Nat. Methods* **14,** 979–982 (2017).

28. Eden, E., Navon, R., Steinfeld, I., Lipson, D. & Yakhini, Z. GOrilla: A tool for discovery and visualization of enriched GO terms in ranked gene lists. *BMC Bioinformatics* **10,** 1–7 (2009).

Supplementary figures

Supplementary Figure 1. Protocol followed to generate ESC-microglia like cells. (**a**) Schematic representation of the protocol and (**b**) quality control (in triplicate) for the microglia differentiation step (in green), showing representative bright field image, flow cytometry data on CD45 and CX3CR1 expression, and mRNA analysis for multiple microglial makers. Graph shows mean±SEM, n=3, one-way ANOVA, * $p<0.05$, ** $p<0.01$, *** $p<0.001$ vs. M-CSF + IL-34.

Supplementary Figure 2. Endogenous mouse microglia depletion. CSF1R inhibitor BLZ945 was administered (200 mg/kg, i.p.) 24 and 48h prior to human microglia transplantation. Scale bar, 100 µm. Graph shows mean±SEM, n=3 mice per group, two-tailed t-test *p=0.002.

Extended Data 1. **Gating strategy for the isolation of H9-microglia from the mouse brain and graft efficiency**. (**a**) Human cells were sorted according to the expression of CD11b, hCD45, and GFP, whereas mouse cells only expressed CD11b but were negative for hCD45 and GFP. (**b**) H9-microglia graft efficiency. Percentage of CD11b cells in the total sample, and proportion of human cells amongst them. Graph shows mean±SEM, n=6 mice per group.

Extended Data 2. H9-microglia showed a widespread distribution across multiple areas of the brain. (**a**) Representative overview of the extent of H9-microglia graft in the mouse brain. Human microglia are stained for P2RY12 across consecutive sections separated by 500µm to capture multiple anatomical areas. Scale bar, 1mm. (**b**) Higher magnification images of multiple anatomical areas including meninges, cortex, striatum, white matter, choroid plexus and hippocampus. Labelling shows DAPI (in blue), GFP (in green) and P2RY12 (in cyan). Images are representative of a staining performed in n=4 mice. Scale bar, 100 µm.

Extended Data 3. Extended clustering and distribution of *in vitro*, *in vivo* (engrafted) H9 and primary microglia. (**a**) PCA shows clear separation between *in vitro* (MNC and MG) and *in vivo* (engrafted H9 and primary) microglia. The colours correspond to the clustering shown in **Figure 2a**. (**b**) t-SNE plots as in **Figure 2a**, coloured by the combined level of expression of groups of

genes that characterise distinct microglial states. The original clusters from **Figure 2a** are outlined. (**c**) Selected genes defining the different transcriptomic scores shown in **b**. The full list of genes is shown in Supplementary Table 3. (**d**) Distribution of the different samples across the tSNE plot, and (**e**) percentage of each sample across the different clusters. All the data shown represents 2,246 transplanted H9-microglia (*in vivo)* (n=3/1, 3 mice in 1 combined sequencing pool), 4496 H9-derived monocytes (n=2/1, 2 differentiations in 1 combined sequencing pool) and 3385 microglia *in vitro* (n=2/1), and 22,846 human primary microglia obtained from cortical surgical resections (n=7/7 online Methods).

Extended Data 4. Direct comparison of *in vitro*, *in vivo* (engrafted) H9 and primary microglia. **(a)** Volcano plots showing paired comparisons between average gene expression *in vitro* MNC, *in vitro* MG, *in vivo* (engrafted) MG and primary cells. (**b**) Individual comparisons of in vivo (engrafted) H9-microglia and each human subject (human cases 1-7). The dashed line corresponds to an arbitrary threshold logFC of 0.2. Blue labels correspond to homeostatic genes whereas red labels correspond to microglial activation genes (Supplementary Table 3). All the data shown represents 2,246 transplanted H9-microglia (*in vivo)* (n=3/1, 3 mice in 1 combined sequencing pool), 4496 H9-derived monocytes (n=2/1, 2 differentiations in 1 combined sequencing pool) and 3385 microglia *in vitro* (n=2/1), and 22,846 human primary microglia obtained from cortical surgical resections (n=7/7). In all cases, Wilcoxon Rank Sum test, *p-values* adjusted with Bonferroni correction based on the total number of genes in the dataset.

Extended Data 5. Characterization of oAβ preparation. Freshly eluted recombinant Aβ1-42 monomers follow a rapid aggregation course in Tris-EDTA buffer. (**a**) After 2 hours of incubation, Aβ1-42 monomers oligomerize and run as dimers and trimers (indicated with *) on SDS-PAGE/Coomassie staining, and they are proteinase-K sensitive. (**b**) Early Aβ1-42 oligomers form A11 and OC-positive aggregates. Two µl of either scrambled or amyloid beta 1-42 from different time points (0 hours, 2 hours and 2 weeks) of incubation was spotted on blots. These dot blots were probed with A11 antibody (Invitrogen; #AHB0052), which recognizes amino acid sequence-independent oligomers of proteins or peptides. A11 epitope is transient and is present only in the early oligomers (2 h), in contrast to the mature fibers (2 w) formed after 2 weeks of incubation. No fibrillary material is detected after 2 hours of incubation. (**c**) OC antibody (Millipore; #AB2286) recognize epitopes common to monomers, amyloid oligomers, and fibrils. (**d**) 4G8 antibody

(Eurogentec; #SIG-39220) detects N-terminal of the amyloid aggregates (epitope between amino acids 17-24).

Extended Data 6. Preparation of the datasets for the analysis of (a-c) host mouse and (d-f) H9-microglia response to oAβ (see Figure 3). (a) t-SNE plot of the 13342 cells passing quality control, coloured by clusters. (**b**) t-SNE plots as in **a**, coloured by the level of ln normalized expression of selected genes for microglia (*Cx3cr1*, *Tmem119*), monocytes (*Ccr2*) and neutrophils (*Ccrl2*). (**c**) Violin plots of selected marker genes for homeostatic microglia (*Cx3cr1*, *Tmem119*), CRM (*Il1b*), ARM (*Cd74*, *H2-Eb1*, *Ifit3*), neutrophils (*Ccrl2*), monocytes (*Ccr2*, *Ly6c1*), astrocytes (*Clu*), oligodendrocytes (*Mbp*), neurons (*Npy*), and cycling cells (*Top2a*). Analysis shown in **Figure 2** was performed after removal of clusters 4 (neutrophils), 7 (monocytes), 10 (astrocytes), 12 (oligodendrocytes) and 9 (neurons). **(d)** t-SNE plot of the 6444 H9-microglia cells passing quality control, coloured by clusters. (**e**) t-SNE plot as in **a**, coloured by treatment (naïve; scrambled peptide, Scr; and oligomeric Aβ, oAβ). (**f**) t-SNE plot as in a, coloured by the level of ln normalized expression of selected genes for microglia (*CX3CR1*), cycling cells (*MKI67*) and brain resident macrophages (*MRC1*, *CD163*). Analysis shown in **Figure 2** was performed after removal of clusters 1 and 4 (brain resident macrophages), 6 (cycling cells) and 8 (doublets).

Extended Data 7. Expanded analysis, clustering and trajectory inference of the analysis of the response of H9-microglia upon oAβ. (**a**) PCA of 4880 H9-microglia isolated from the mouse brain (n=3 mice in 1 combined sequencing pool) shows clear separation of the different clusters identified in our analysis in PC1 and PC2. (**b**) t-SNE plots as in **Figure 3a**, coloured by the combined level of expression of groups of genes that characterise distinct microglial states. (**c**) Selected genes defining the different transcriptomic scores shown in **Figure 3b**: homeostatic score (1), cytokine score (2) activated score (3). The full list of genes is shown in Supplementary Table 3. (**d**) Volcano plots showing paired comparisons between H9.HM, H9.CRM and H9.PM clusters ((Wilcoxon Rank Sum test, *p-values* adjusted with Bonferroni correction based on the total number of genes in the dataset). (**e**) Proportion of the different experimental groups across clusters in **Figure 3a (**Chi^2 test, *** $p < 10^{-250}$). (**f, g**) Phenotypic trajectory inferred by Monocle 2 as shown in **Figure 3a**, coloured by (**f**) treatment and (**g**) clusters from **Figure 3a**.

Extended Data 8. Expanded analysis, clustering and trajectory inference of the analysis of the response of mouse host microglia upon oAβ. (**a**) PCA of 9942 endogenous mouse cells (n=3 mice in 1 combined sequencing pool) shows clear separation of the different clusters identified in our analysis in PC1 and PC2. (**b**) t-SNE plots as in **Figure 3d**, coloured by the combined level of expression of groups of genes that characterise distinct microglial states. (**c**) Selected genes defining the different transcriptomic scores shown in **b**: homeostatic score (1), cytokine score (2) activated score (3). The full list of genes is shown in Supplementary Table 3. (**d**) Volcano plots showing paired comparisons between ms.HM, ms.CRM and ms.ARM clusters (Wilcoxon Rank Sum test, *p-values* adjusted with Bonferroni correction based on the total number of genes in the dataset). (**e**) Proportion of the different experimental groups across clusters in **Figure 3d (**Chi^2 test, *** $p < 10^{-250}$). (**f, g**) Phenotypic trajectory inferred by Monocle 2 as shown in **Figure 3c**, coloured by (**f**) treatment and (**g**) clusters from **Figure 3d**.

Extended Data 9. Cytokine response microglia (CRM) are also present in APP^{NL-G-F} mice. (**a**) Original clustering analysis from Sala Frigerio et al. (2019)[11] consisting of 10,801 microglial cells from 3 to 21 months old APP^{NL-G-F} mice and aged matched wild type controls. (**b**) Clusters shown in **a**, coloured with CRM, HM, ARM and IRM transcriptomic signatures. Note the small population of cells displaying CRM features embeded into the ARM response in APP^{NL-G-F} microglia. (**c**) Significant enrichment of either homeostatic (HM) or activated (ARM) microglia gene sets from Sala Frigerio et al. (2019)[11] in our ms.HM and ms.ARM clusters, respectively (ANOVA with Turkey HSD multiple comparisons correction, *** $p \approx 0$; box plots represent median, with 25^{th} and 75^{th} percentiles and 1.5 times the inter-quartile range as minima and maxima). (**d**) Subselection of CRM cells from the main clusters shown in **a**. (**e**) Microglia cells enriched with a CRM transcriptomic profile are largely located at early stages of the response to amyloid in APP^{NL-G-F} mice[11]. The left panel shows the trajectory analysis coloured by clusters as represented in panel **a**, whereas the right panel highlights the cells displaying a CRM profile.

Extended Data 10. Differential responses of human and host mouse microglia to oligomeric Aβ. (**a**) Pathway enrichment analysis (GOrilla) shows that the differentially expressed genes in CRM vs. HM clusters are involved in immune and inflammatory processes. (**b)** Top differentially expressed genes in H9-microglia upon Aβ challenge relative to scrambled peptide, and expression of their mouse orthologs by endogenous mouse cells. Coloured marks indicate the functional

category as shown in **b**. (**c**) Differentially expressed genes that show opposite behaviour in H9- and mouse host (*Rag2*$^{-/-}$ *Il2rγ*$^{-/-}$) microglia. Coloured marks indicate the functional category as shown in **b**. (**d**) Volcano plots showing paired comparisons between H9.HM, H9.CRM, but including all genes (even those with no clear orthology to mouse, Wilcoxon Rank Sum test, *p-values* adjusted with Bonferroni correction based on the total number of genes in the dataset). (**e**) Further pathway enrichment analysis (GOrilla) performed on the human-specific (with no clear orthology) differentially expressed genes in H9.CRM vs. H9.HM clusters are involved in cytokine/chemokine responses.

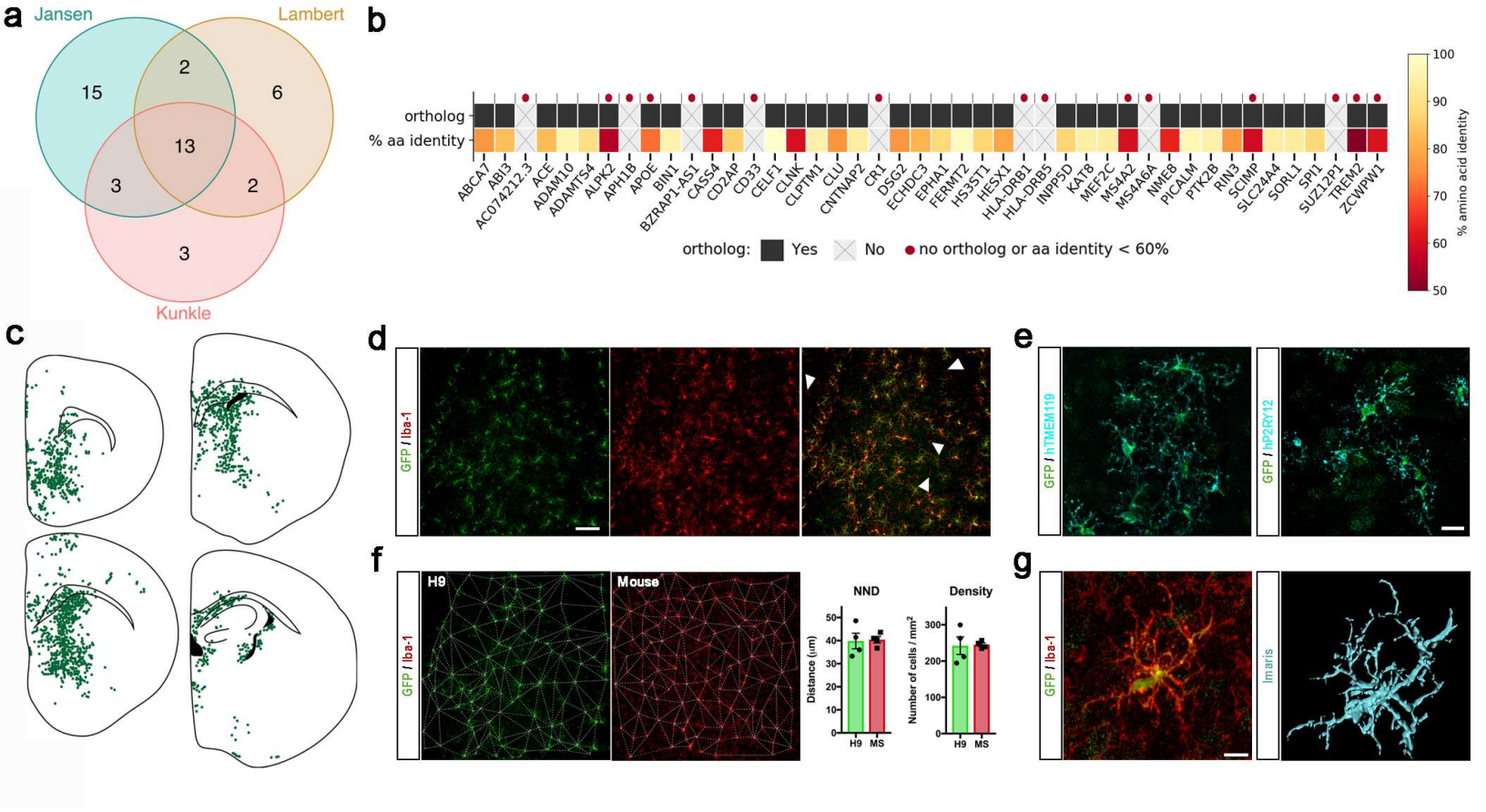
a
Jansen
Lambert
Kunkle
15
2
6
13
3
2
3
b
ortholog
% aa identity
ABCA7
ABI3
AC074212.3
ACE
ADAM10
ADAMTS4
ALPK2
APH1B
APOE
BIN1
BZRAP1-AS1
CASS4
CD2AP
CD33
CELF1
CLNK
CLPTM1
CLU
CNTNAP2
CR1
DSG2
ECHDC3
EPHA1
FERMT2
HS3ST1
HESX1
HLA-DRB1
HLA-DRB5
INPP5D
KAT8
MEF2C
MS4A2
MS4A6A
NME8
PICALM
PTK2B
RIN3
SCIMP
SLC24A4
SORL1
SPI1
SUZ12P1
TREM2
ZCWPW1
ortholog: Yes No no ortholog or aa identity < 60%
100
90
80
70
60
50
% amino acid identity
c
d
GFP / Iba-1
e
GFP / hTMEM119
GFP / hP2RY12
f
H9
Mouse
GFP / Iba-1
NND
Distance (um)
50
40
30
20
10
0
H9
MS
Density
Number of cells / mm²
300
200
100
0
H9
MS
g
GFP / Iba-1
Imaris

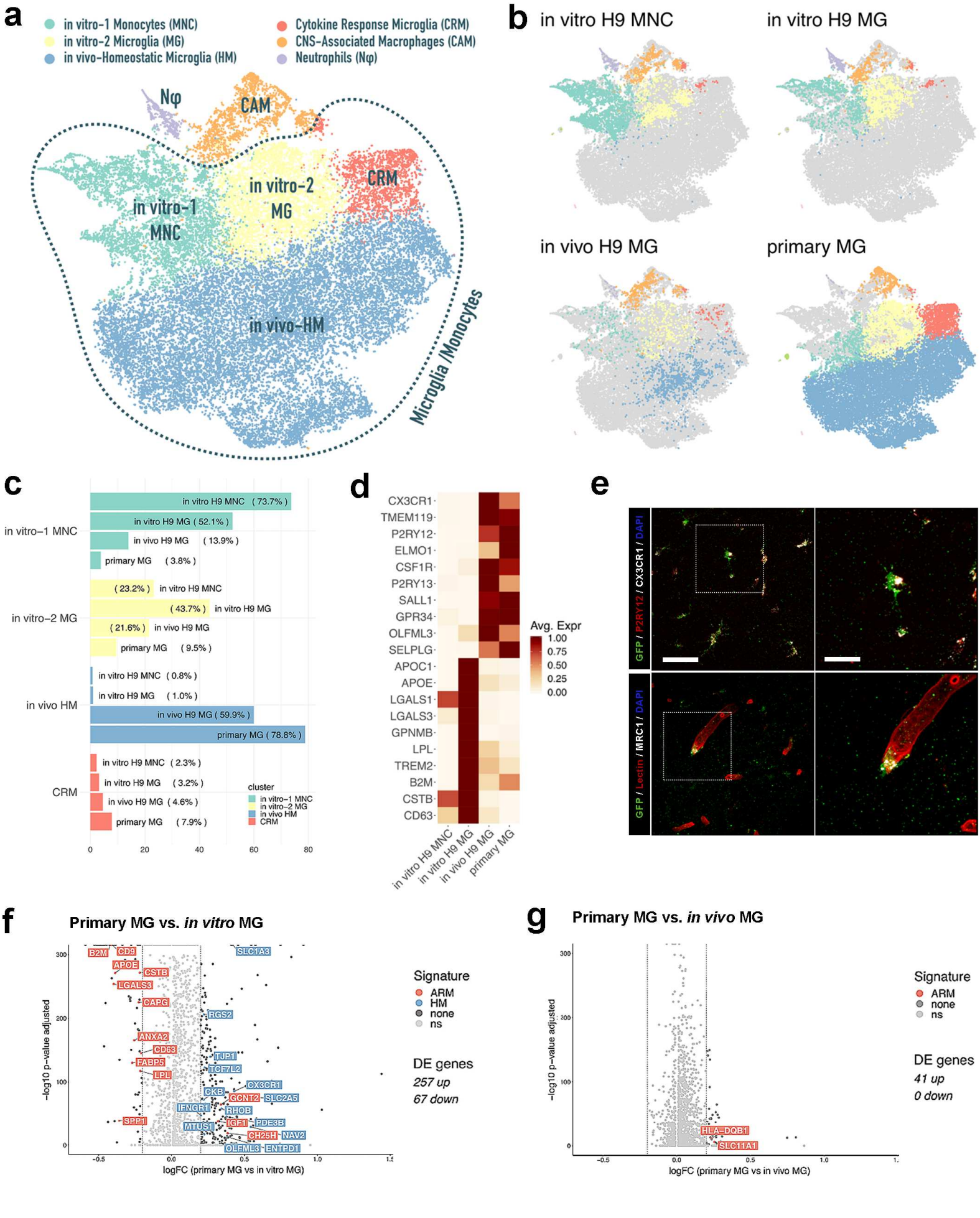
a
in vitro-1 Monocytes (MNC)
in vitro-2 Microglia (MG)
in vivo-Homeostatic Microglia (HM)
Cytokine Response Microglia (CRM)
CNS-Associated Macrophages (CAM)
Neutrophils (Nφ)
Nφ
CAM
CRM
in vitro-2 MG
in vitro-1 MNC
in vivo-HM
Microglia /Monocytes
b
in vitro H9 MNC
in vitro H9 MG
in vivo H9 MG
primary MG
c
in vitro−1 MNC
in vitro H9 MNC (73.7%)
in vitro H9 MG (52.1%)
in vivo H9 MG (13.9%)
primary MG (3.8%)
in vitro−2 MG
(23.2%) in vitro H9 MNC
(43.7%) in vitro H9 MG
(21.6%) in vivo H9 MG
primary MG (9.5%)
in vivo HM
in vitro H9 MNC (0.8%)
in vitro H9 MG (1.0%)
in vivo H9 MG (59.9%)
primary MG (78.8%)
CRM
in vitro H9 MNC (2.3%)
in vitro H9 MG (3.2%)
in vivo H9 MG (4.6%)
primary MG (7.9%)
cluster
in vitro−1 MNC
in vitro−2 MG
in vivo HM
CRM
0
20
40
60
80
d
CX3CR1
TMEM119
P2RY12
ELMO1
CSF1R
P2RY13
SALL1
GPR34
OLFML3
SELPLG
APOC1
APOE
LGALS1
LGALS3
GPNMB
LPL
TREM2
B2M
CSTB
CD63
Avg. Expr
1.00
0.75
0.50
0.25
0.00
in vitro H9 MNC
in vitro H9 MG
in vivo H9 MG
primary MG
e
GFP / P2RY12 / CX3CR1 / DAPI
GFP / Lectin / MRC1 / DAPI
f
Primary MG vs. in vitro MG
−log10 p−value adjusted
logFC (primary MG vs in vitro MG)
B2M
CD9
APOE
CSTB
LGALS3
CAPG
RGS2
ANXA2
CD63
FABP5
LPL
TUBB1
TCF7L2
CX3CR1
CKB
GCNT2
SLC2A5
IFNGR1
RHOB
SPP1
IGF1
PDE3B
MTUS1
CH25H
NAV2
OLFML3
ENTPD1
SLC1A3
Signature
ARM
HM
none
ns
DE genes
257 up
67 down
g
Primary MG vs. in vivo MG
−log10 p−value adjusted
logFC (primary MG vs in vivo MG)
HLA-DQB1
SLC11A1
Signature
ARM
none
ns
DE genes
41 up
0 down

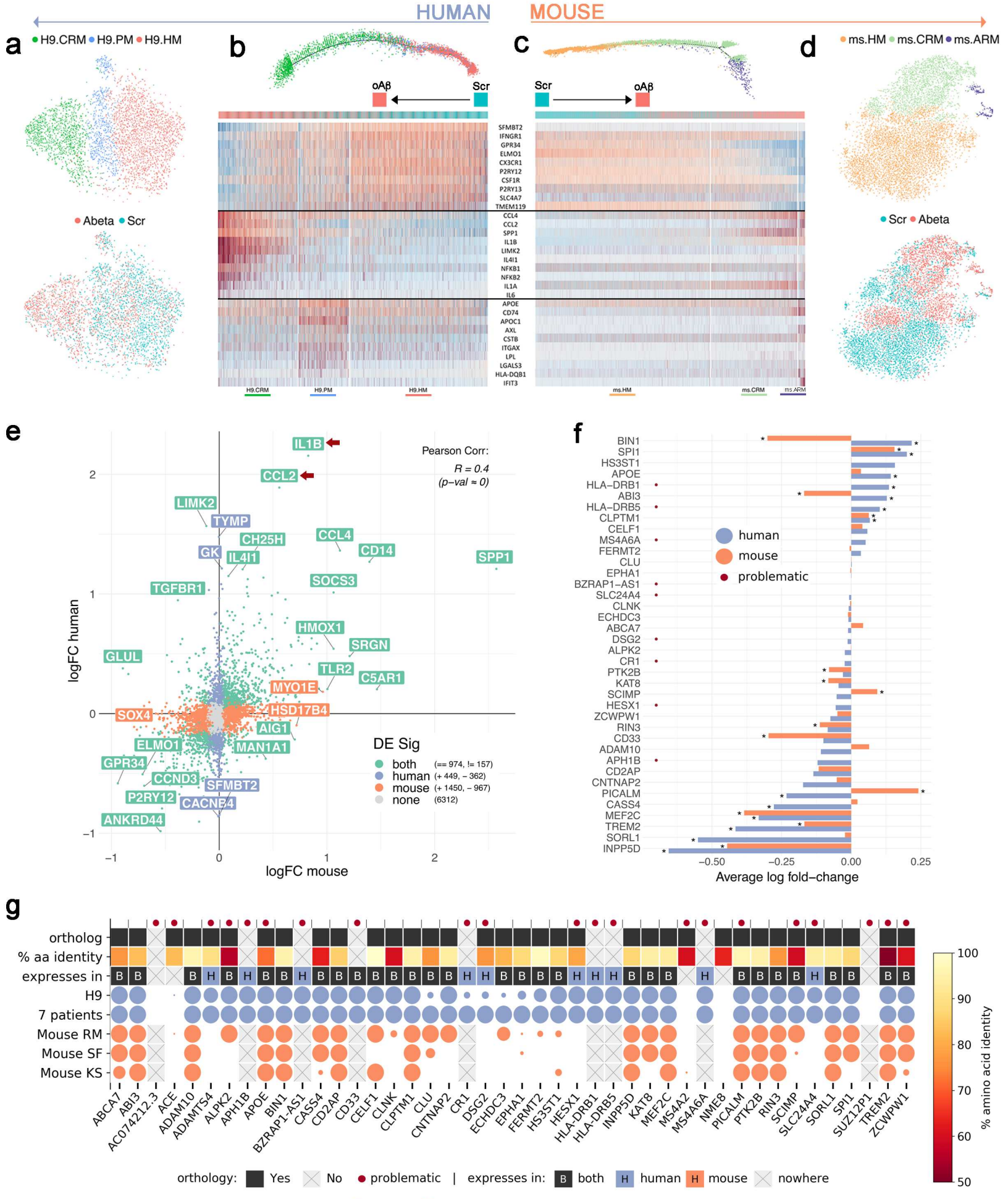
HUMAN
MOUSE
a
H9.CRM H9.PM H9.HM
Abeta Scr
b
oAβ
Scr
SFMBT2
IFNGR1
GPR34
ELMO1
CX3CR1
P2RY12
CSF1R
P2RY13
SLC4A7
TMEM119
CCL4
CCL2
SPP1
IL1B
LIMK2
IL4I1
NFKB1
NFKB2
IL1A
IL6
APOE
CD74
APOC1
AXL
CSTB
ITGAX
LPL
LGALS3
HLA-DQB1
IFIT3
H9.CRM
H9.PM
H9.HM
c
Scr
oAβ
ms.HM
ms.CRM
ms.ARM
d
ms.HM ms.CRM ms.ARM
Scr Abeta
e
Pearson Corr:
R = 0.4
(p–val ≈ 0)
IL1B
CCL2
LIMK2
TYMP
CH25H
CCL4
CD14
GK
IL4I1
SPP1
SOCS3
TGFBR1
HMOX1
SRGN
GLUL
TLR2
C5AR1
MYO1E
SOX4
HSD17B4
AIG1
ELMO1
MAN1A1
GPR34
CCND3
SFMBT2
P2RY12
CACNB4
ANKRD44
DE Sig
both (== 974, != 157)
human (+ 449, – 362)
mouse (+ 1450, – 967)
none (6312)
logFC human
logFC mouse
f
BIN1
SPI1
HS3ST1
APOE
HLA–DRB1
ABI3
HLA–DRB5
CLPTM1
CELF1
MS4A6A
FERMT2
CLU
EPHA1
BZRAP1–AS1
SLC24A4
CLNK
ECHDC3
ABCA7
DSG2
ALPK2
CR1
PTK2B
KAT8
SCIMP
HESX1
ZCWPW1
RIN3
CD33
ADAM10
APH1B
CD2AP
CNTNAP2
PICALM
CASS4
MEF2C
TREM2
SORL1
INPP5D
human
mouse
problematic
Average log fold–change
g
ortholog
% aa identity
expresses in
H9
7 patients
Mouse RM
Mouse SF
Mouse KS
ABCA7 ABI3 AC074212.3 ACE ADAM10 ADAMTS4 ALPK2 APH1B APOE BIN1 BZRAP1-AS1 CASS4 CD2AP CD33 CELF1 CLNK CLPTM1 CLU CNTNAP2 CR1 DSG2 ECHDC3 EPHA1 FERMT2 HS3ST1 HESX1 HLA-DRB1 HLA-DRB5 INPP5D KAT8 MEF2C MS4A2 MS4A6A NME8 PICALM PTK2B RIN3 SCIMP SLC24A4 SORL1 SPI1 SUZ12P1 TREM2 ZCWPW1
% amino acid identity
orthology: Yes No problematic | expresses in: both human mouse nowhere
single cell expression: human mouse | expresses in: >= 100: 50: 10: cells

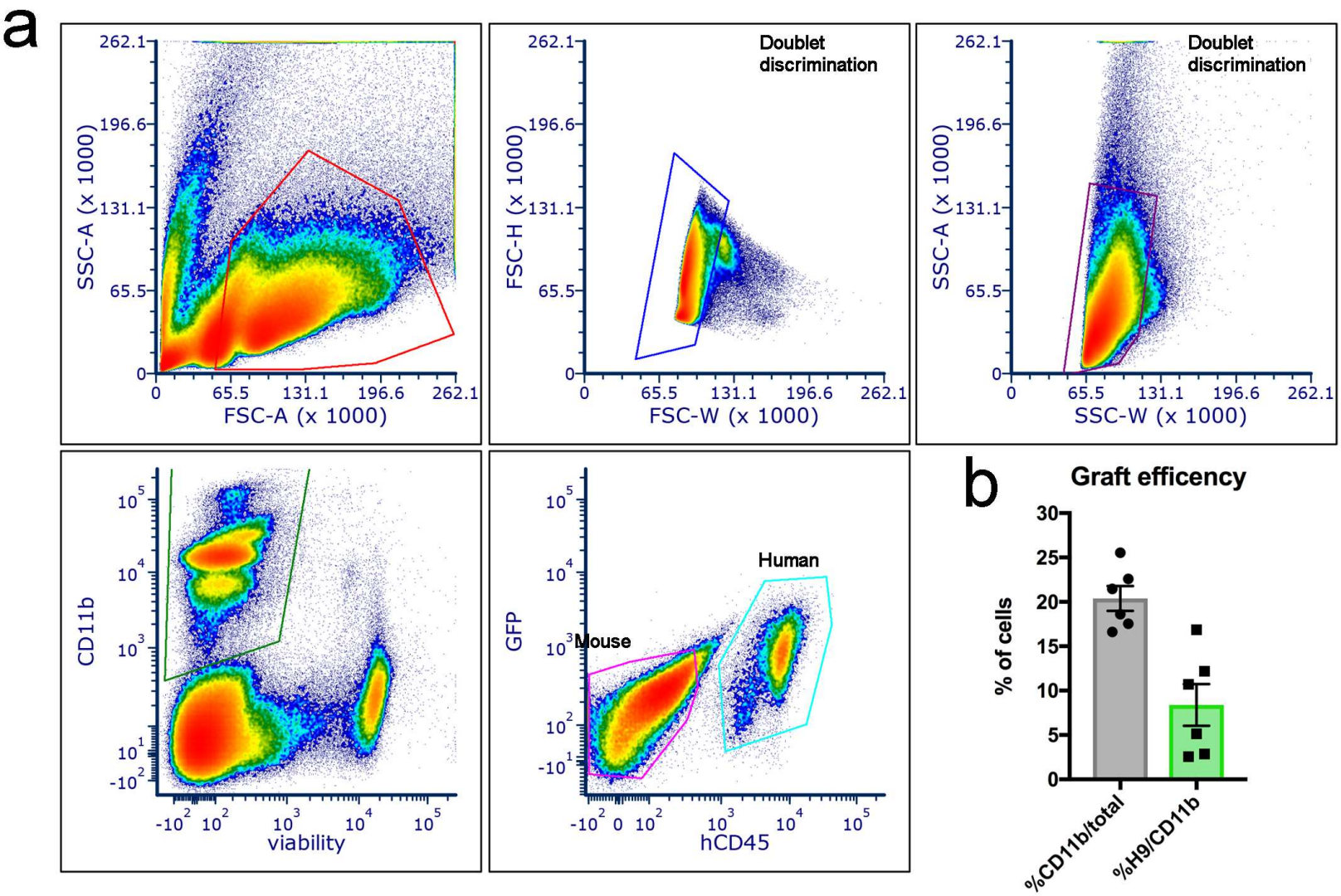
a
SSC-A (x 1000)
FSC-A (x 1000)
Doublet discrimination
FSC-H (x 1000)
FSC-W (x 1000)
Doublet discrimination
SSC-A (x 1000)
SSC-W (x 1000)
CD11b
viability
GFP
Mouse
Human
hCD45
b
Graft efficency
% of cells
%CD11b/total
%H9/CD11b

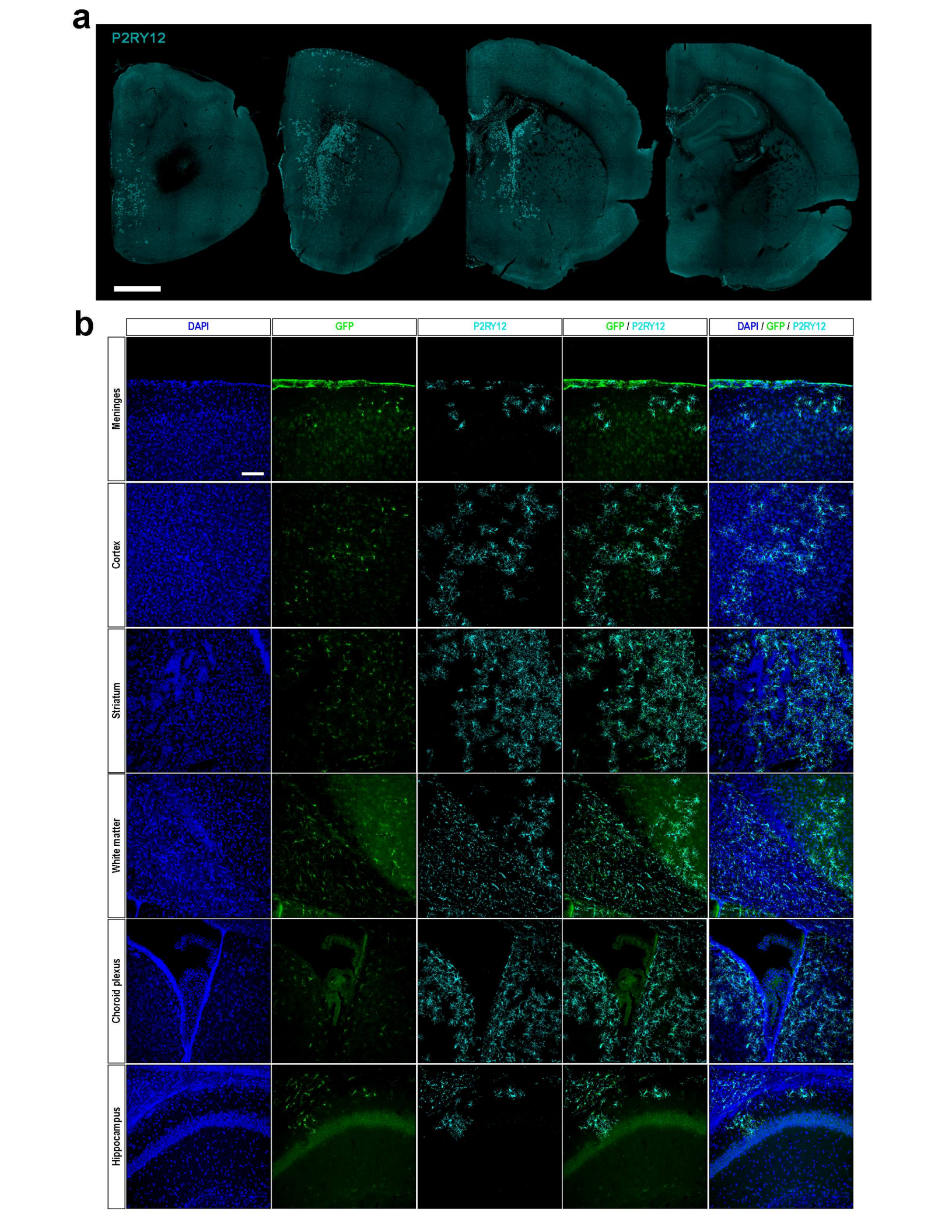
a
P2RY12
b
DAPI
GFP
P2RY12
GFP / P2RY12
DAPI / GFP / P2RY12
Meninges
Cortex
Striatum
White matter
Choroid plexus
Hippocampus

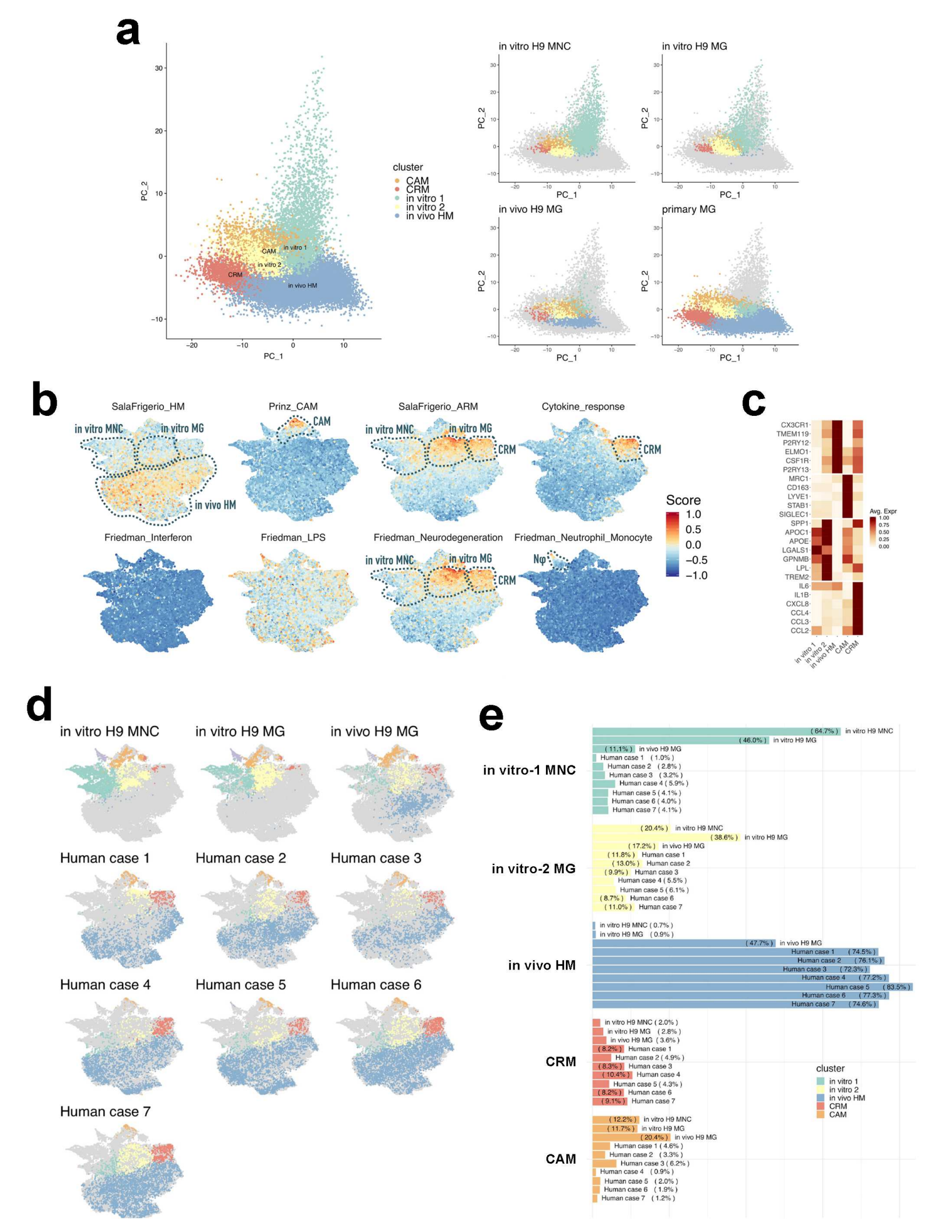
a
cluster
CAM
CRM
in vitro 1
in vitro 2
in vivo HM
PC_1
PC_2
in vitro H9 MNC
in vitro H9 MG
in vivo H9 MG
primary MG
b
SalaFrigerio_HM
Prinz_CAM
SalaFrigerio_ARM
Cytokine_response
Friedman_Interferon
Friedman_LPS
Friedman_Neurodegeneration
Friedman_Neutrophil_Monocyte
Score
1.0
0.5
0.0
−0.5
−1.0
c
CX3CR1
TMEM119
P2RY12
ELMO1
CSF1R
P2RY13
MRC1
CD163
LYVE1
STAB1
SIGLEC1
SPP1
APOC1
APOE
LGALS1
GPNMB
LPL
TREM2
IL6
IL1B
CXCL8
CCL4
CCL3
CCL2
Avg. Expr
d
Human case 1
Human case 2
Human case 3
Human case 4
Human case 5
Human case 6
Human case 7
e
in vitro-1 MNC
in vitro-2 MG
in vivo HM
CRM
CAM
cluster

a

Primary MG vs. *in vitro* MNC

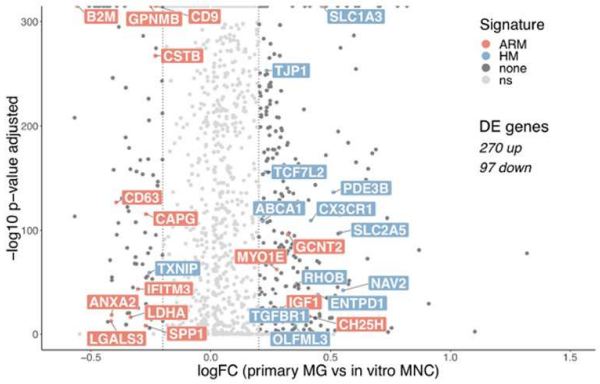

In vivo MG vs. *in vitro* MNC

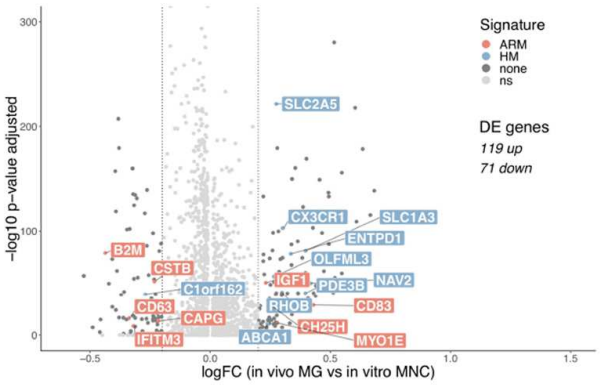

In vivo MG vs. *in vitro* MG

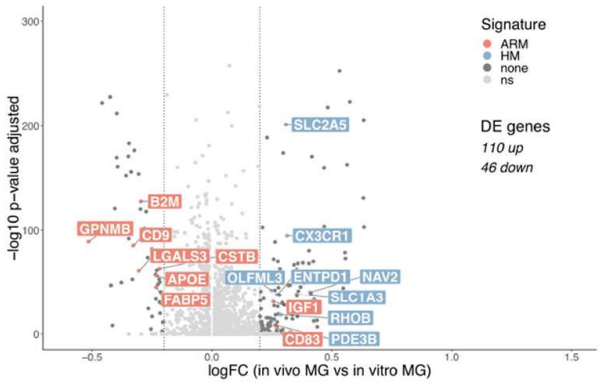

In vitro MG vs. *in vitro* MNC

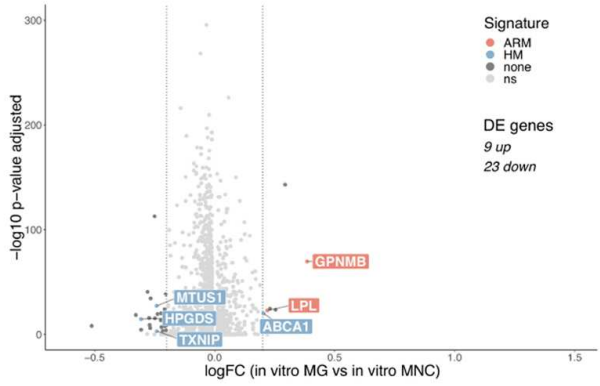

b

Human case 1 vs. *in vivo* MG

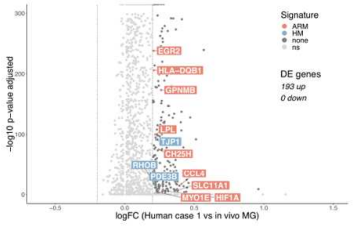

Human case 3 vs. *in vivo* MG

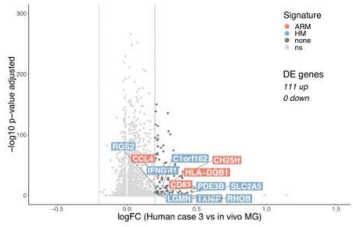

Human case 5 vs. *in vivo* MG

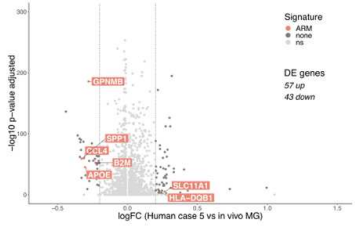

Human case 7 vs. *in vivo* MG

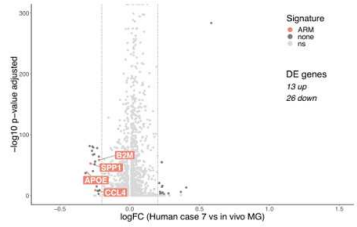

Human case 2 vs. *in vivo* MG

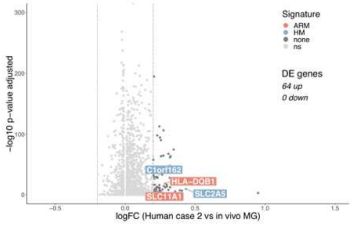

Human case 4 vs. *in vivo* MG

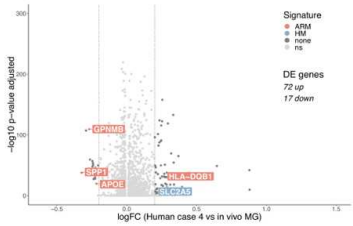

Human case 6 vs. *in vivo* MG

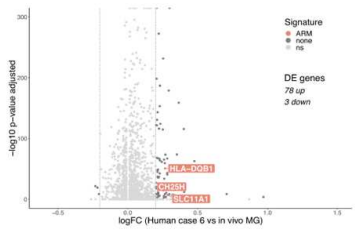

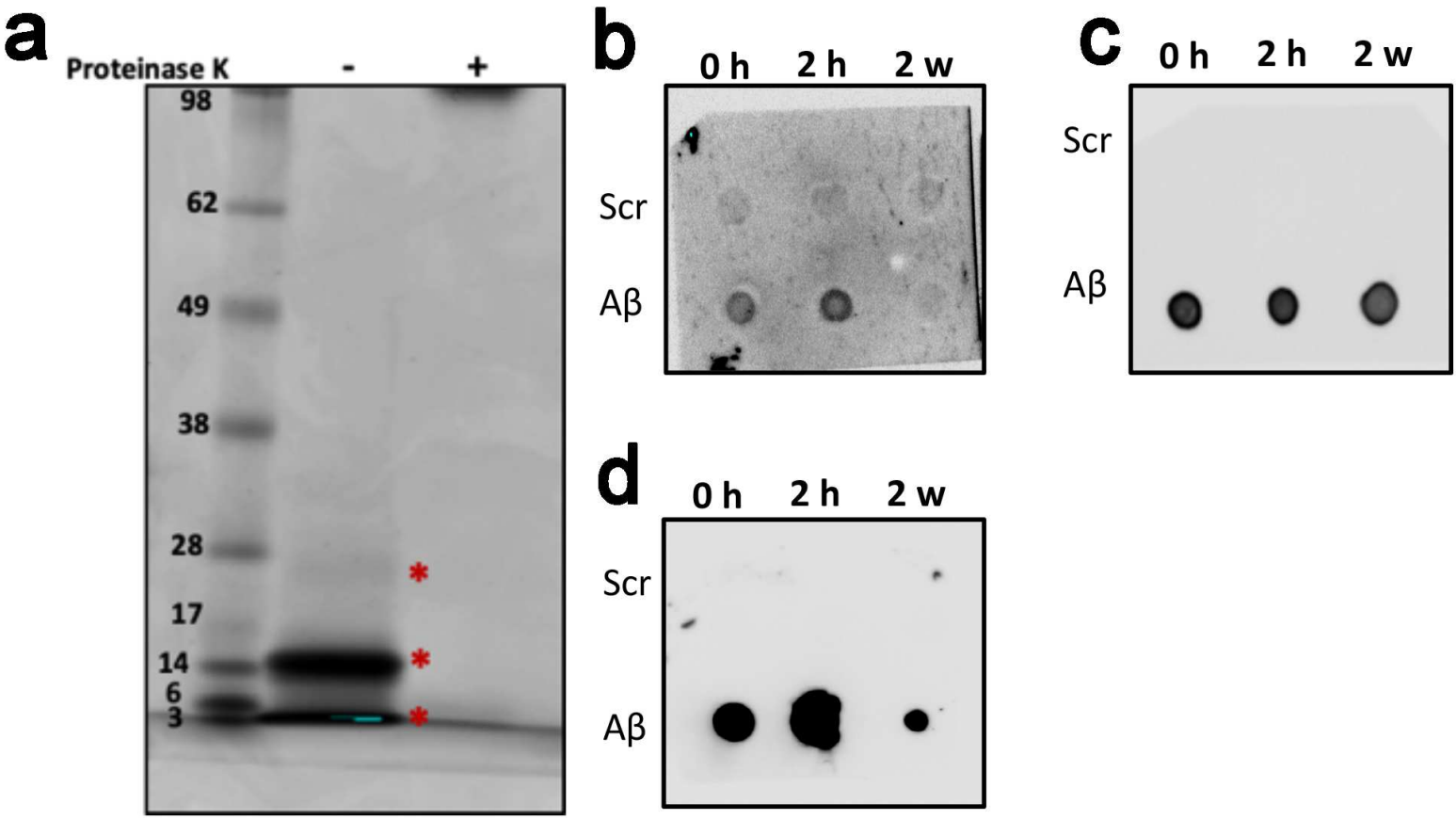
a
Proteinase K
-
+
98
62
49
38
28
17
14
6
3
b
0 h
2 h
2 w
Scr
Aβ
c
0 h
2 h
2 w
Scr
Aβ
d
0 h
2 h
2 w
Scr
Aβ

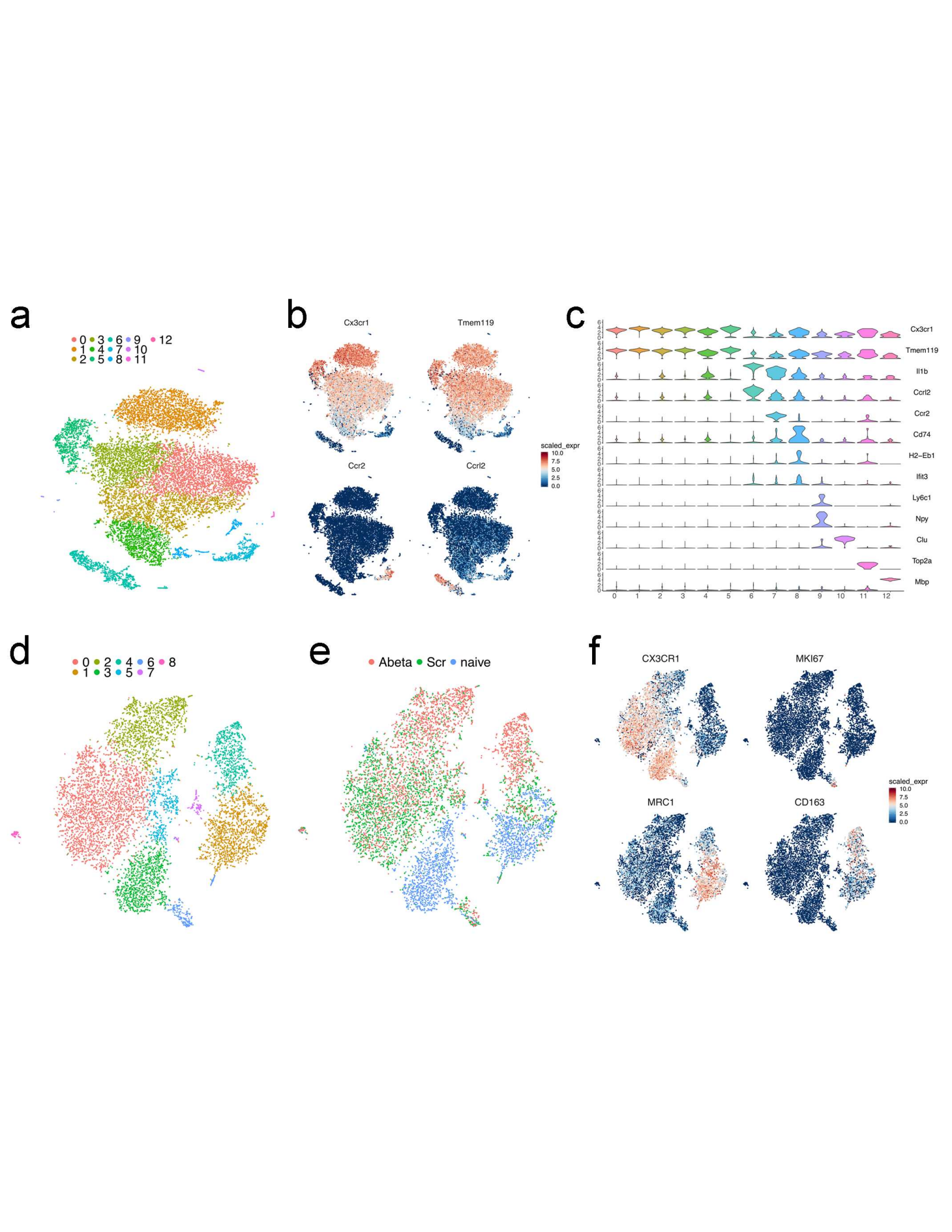
a
0 3 6 9 12
1 4 7 10
2 5 8 11
b
Cx3cr1
Tmem119
Ccr2
Ccrl2
scaled_expr
10.0
7.5
5.0
2.5
0.0
c
Cx3cr1
Tmem119
Il1b
Ccrl2
Ccr2
Cd74
H2−Eb1
Ifit3
Ly6c1
Npy
Clu
Top2a
Mbp
0 1 2 3 4 5 6 7 8 9 10 11 12
d
0 2 4 6 8
1 3 5 7
e
Abeta Scr naive
f
CX3CR1
MKI67
MRC1
CD163
scaled_expr
10.0
7.5
5.0
2.5
0.0

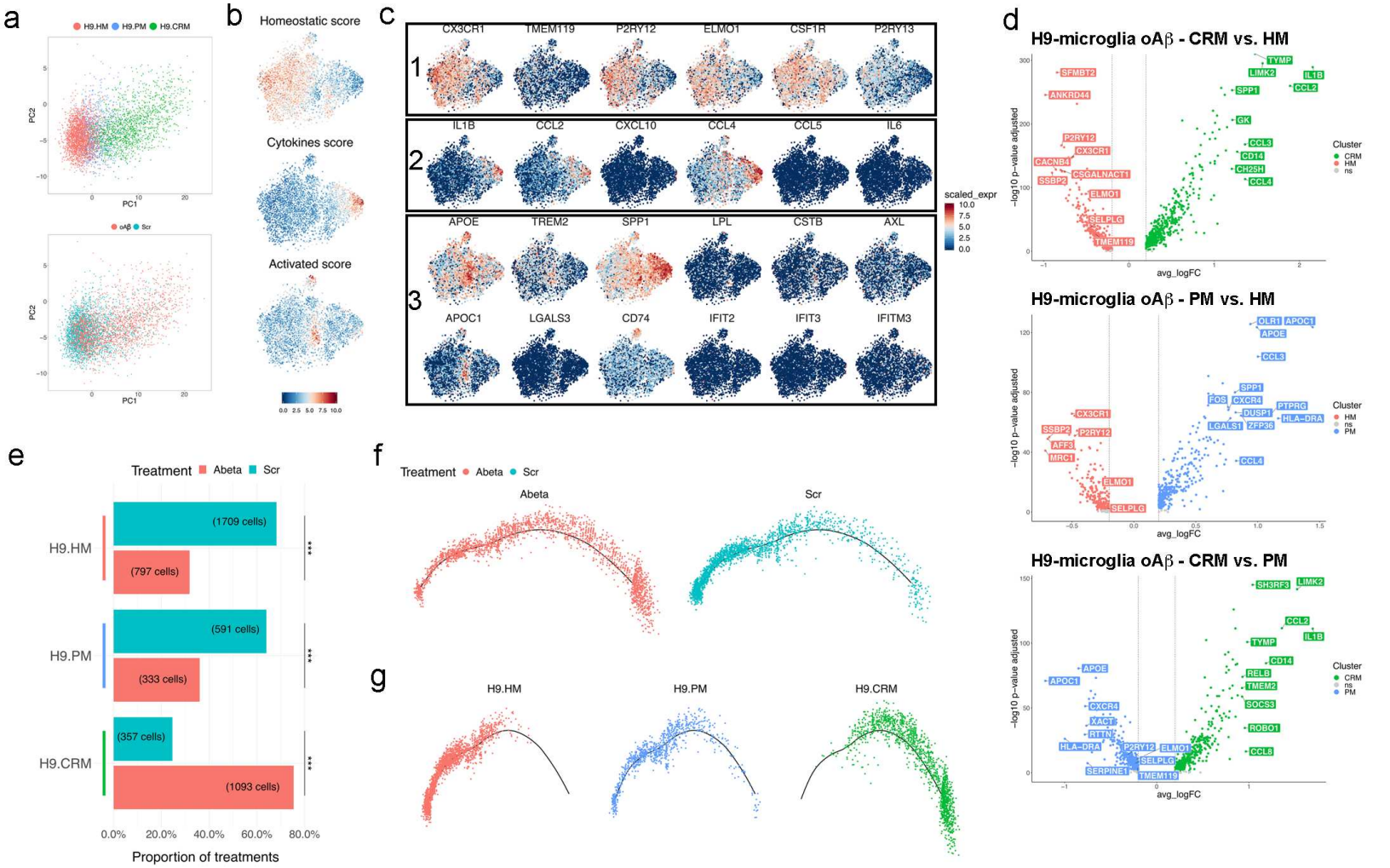
a
H9.HM H9.PM H9.CRM
PC1
PC2
oAβ Scr
b
Homeostatic score
Cytokines score
Activated score
c
CX3CR1 TMEM119 P2RY12 ELMO1 CSF1R P2RY13
IL1B CCL2 CXCL10 CCL4 CCL5 IL6
APOE TREM2 SPP1 LPL CSTB AXL
APOC1 LGALS3 CD74 IFIT2 IFIT3 IFITM3
scaled_expr
d
H9-microglia oAβ - CRM vs. HM
H9-microglia oAβ - PM vs. HM
H9-microglia oAβ - CRM vs. PM
avg_logFC
−log10 p−value adjusted
Cluster
CRM
HM
PM
ns
e
Treatment Abeta Scr
H9.HM
H9.PM
H9.CRM
(1709 cells)
(797 cells)
(591 cells)
(333 cells)
(357 cells)
(1093 cells)
Proportion of treatments
f
Treatment Abeta Scr
Abeta
Scr
g
H9.HM
H9.PM
H9.CRM

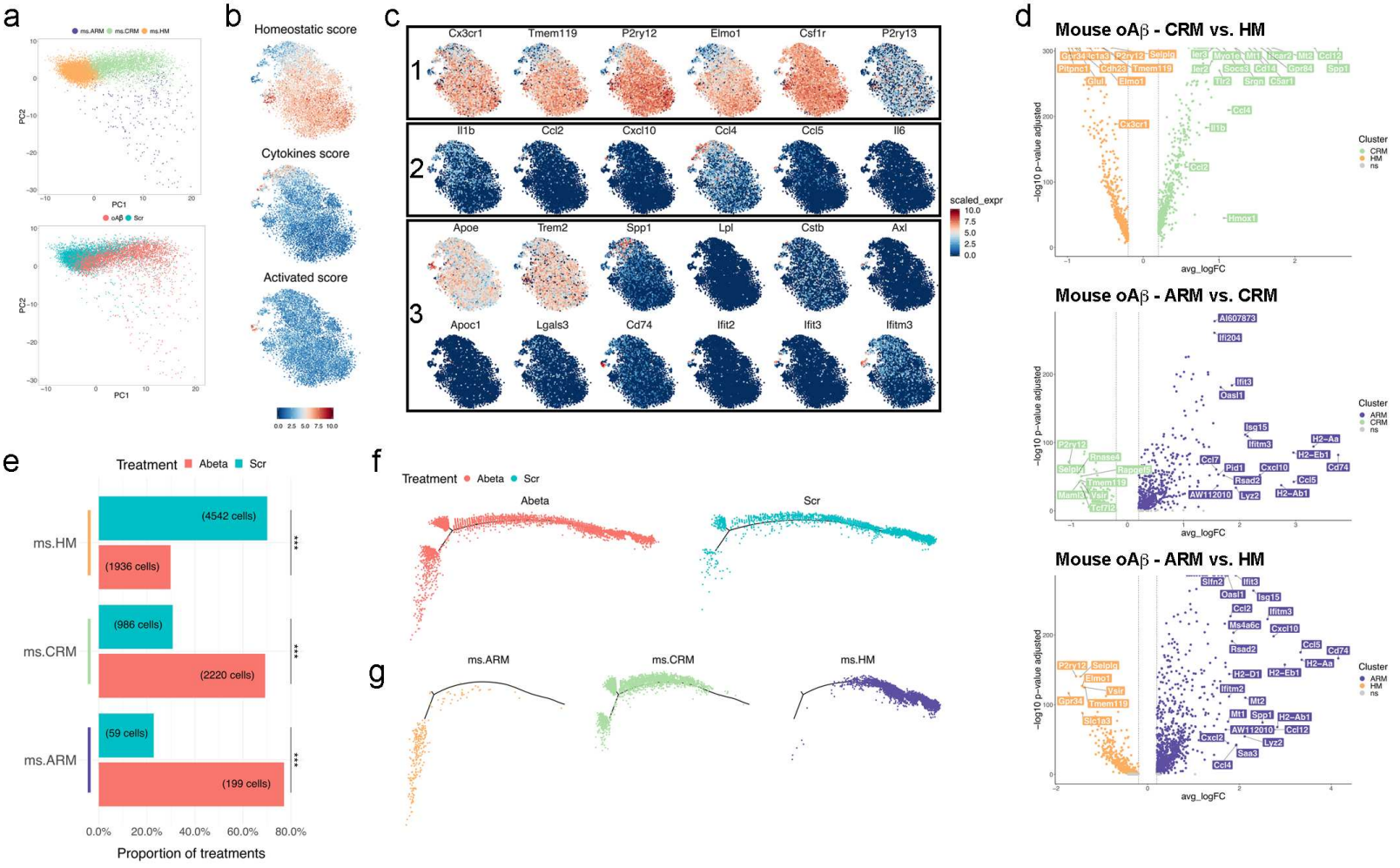
a
ms.ARM ms.CRM ms.HM
PC2
PC1
oAβ Scr
b
Homeostatic score
Cytokines score
Activated score
0.0 2.5 5.0 7.5 10.0
c
1
Cx3cr1 Tmem119 P2ry12 Elmo1 Csf1r P2ry13
2
Il1b Ccl2 Cxcl10 Ccl4 Ccl5 Il6
3
Apoe Trem2 Spp1 Lpl Cstb Axl
Apoc1 Lgals3 Cd74 Ifit2 Ifit3 Ifitm3
scaled_expr
10.0
7.5
5.0
2.5
0.0
d
Mouse oAβ - CRM vs. HM
Mouse oAβ - ARM vs. CRM
Mouse oAβ - ARM vs. HM
−log10 p-value adjusted
avg_logFC
Cluster
CRM
HM
ARM
ns
e
Treatment Abeta Scr
ms.HM
ms.CRM
ms.ARM
(4542 cells)
(1936 cells)
(986 cells)
(2220 cells)
(59 cells)
(199 cells)
***
0.0% 20.0% 40.0% 60.0% 80.0%
Proportion of treatments
f
Treatment Abeta Scr
Abeta
Scr
g
ms.ARM
ms.CRM
ms.HM

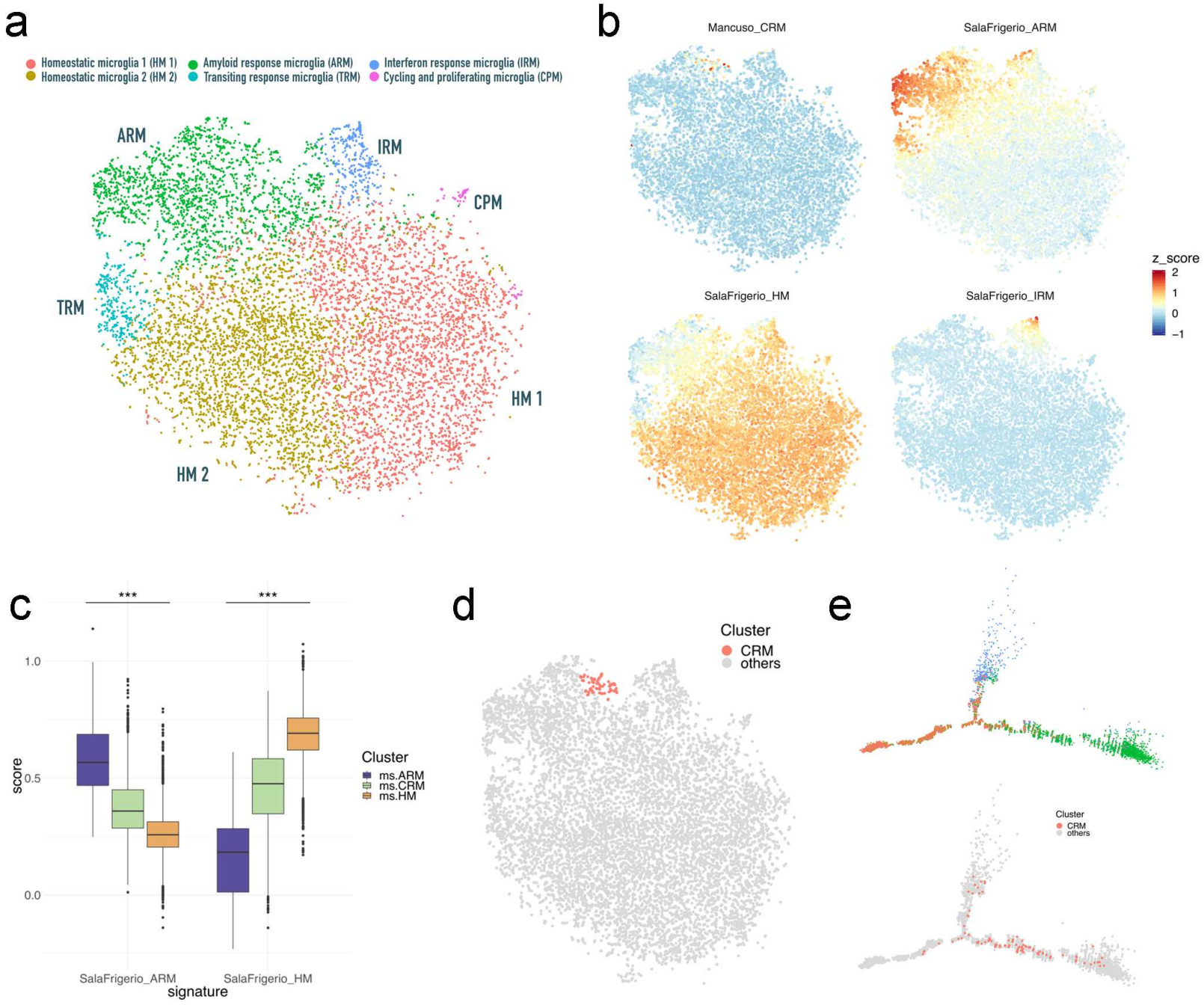
a
Homeostatic microglia 1 (HM 1)
Homeostatic microglia 2 (HM 2)
Amyloid response microglia (ARM)
Transiting response microglia (TRM)
Interferon response microglia (IRM)
Cycling and proliferating microglia (CPM)
ARM
IRM
CPM
TRM
HM 1
HM 2
b
Mancuso_CRM
SalaFrigerio_ARM
SalaFrigerio_HM
SalaFrigerio_IRM
z_score
2
1
0
−1
c
***
***
1.0
0.5
0.0
score
SalaFrigerio_ARM
SalaFrigerio_HM
signature
Cluster
ms.ARM
ms.CRM
ms.HM
d
Cluster
CRM
others
e
Cluster
CRM
others

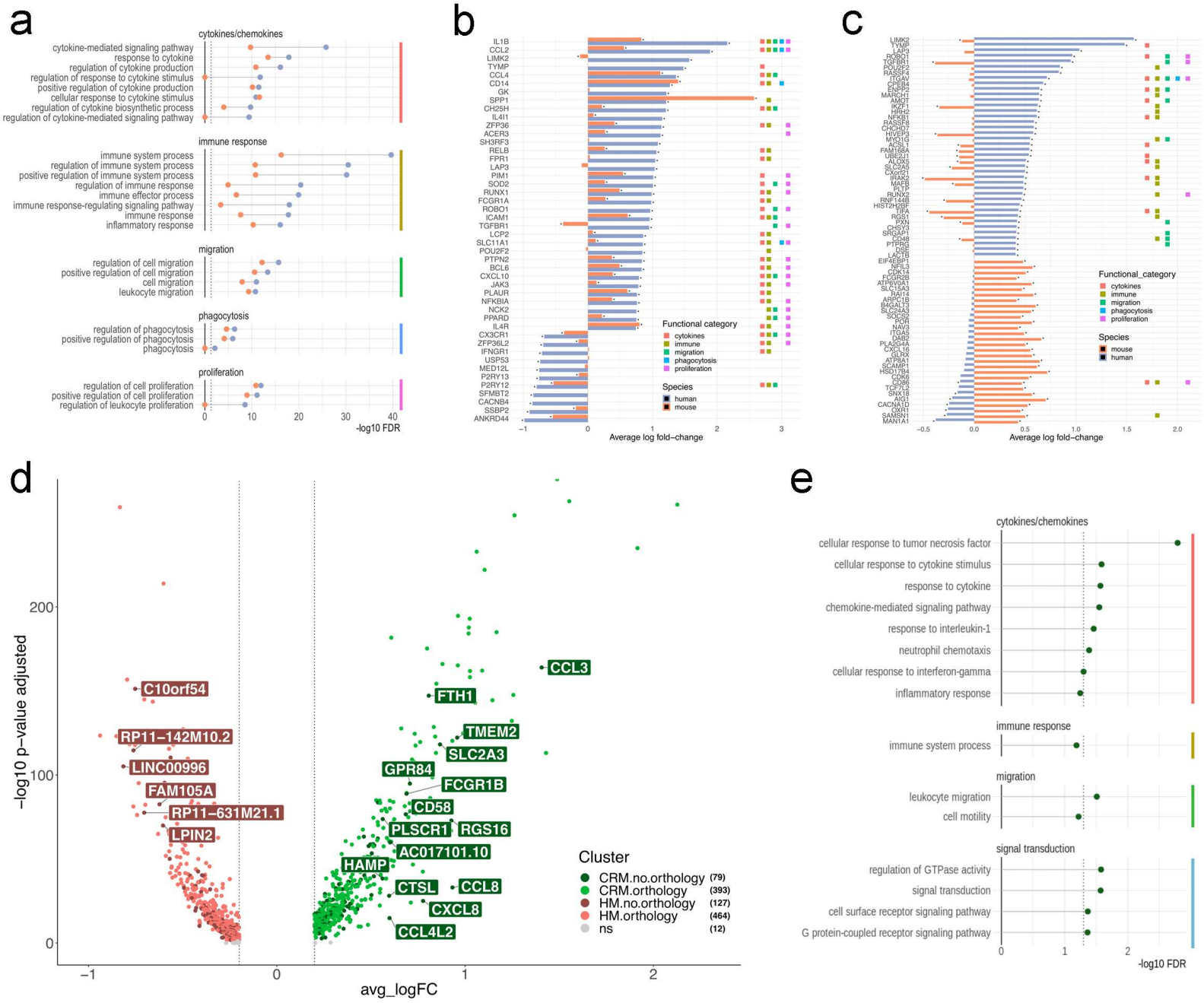
a
cytokines/chemokines
cytokine-mediated signaling pathway
response to cytokine
regulation of cytokine production
regulation of response to cytokine stimulus
positive regulation of cytokine production
cellular response to cytokine stimulus
regulation of cytokine biosynthetic process
regulation of cytokine-mediated signaling pathway
immune response
immune system process
regulation of immune system process
positive regulation of immune system process
regulation of immune response
immune effector process
immune response-regulating signaling pathway
immune response
inflammatory response
migration
regulation of cell migration
positive regulation of cell migration
cell migration
leukocyte migration
phagocytosis
regulation of phagocytosis
positive regulation of phagocytosis
phagocytosis
proliferation
regulation of cell proliferation
positive regulation of cell proliferation
regulation of leukocyte proliferation
0
10
20
30
40
-log10 FDR
b
IL1B
CCL2
LIMK2
TYMP
CCL4
CD14
GK
SPP1
CH25H
IL4I1
ZFP36
ACER3
SH3RF3
RELB
FPR1
LAP3
PIM1
SOD2
RUNX1
FCGR1A
ROBO1
ICAM1
TGFBR1
LCP2
SLC11A1
POU2F2
PTPN2
BCL6
CXCL10
JAK3
PLAUR
NFKBIA
NCK2
PPARD
IL4R
CX3CR1
ZFP36L2
IFNGR1
USP53
MED12L
P2RY13
P2RY12
SFMBT2
CACNB4
SSBP2
ANKRD44
−1
0
1
2
3
Average log fold−change
Functional category
cytokines
immune
migration
phagocytosis
proliferation
Species
human
mouse
c
Functional_category
cytokines
immune
migration
phagocytosis
proliferation
Species
mouse
human
−0.5
0.0
0.5
1.0
1.5
2.0
Average log fold−change
d
200
100
0
−log10 p−value adjusted
C10orf54
RP11−142M10.2
LINC00996
FAM105A
RP11−631M21.1
LPIN2
CCL3
FTH1
TMEM2
SLC2A3
GPR84
FCGR1B
CD58
PLSCR1
RGS16
AC017101.10
HAMP
CTSL
CCL8
CXCL8
CCL4L2
Cluster
CRM.no.orthology (79)
CRM.orthology (393)
HM.no.orthology (127)
HM.orthology (464)
ns (12)
−1
0
1
2
avg_logFC
e
cytokines/chemokines
cellular response to tumor necrosis factor
cellular response to cytokine stimulus
response to cytokine
chemokine-mediated signaling pathway
response to interleukin-1
neutrophil chemotaxis
cellular response to interferon-gamma
inflammatory response
immune response
immune system process
migration
leukocyte migration
cell motility
signal transduction
regulation of GTPase activity
signal transduction
cell surface receptor signaling pathway
G protein-coupled receptor signaling pathway
0
1
2
-log10 FDR